Submission to the Department of Planning & Infrastructure

Proposed Flyers Creek wind Farm
Blayney Local Government Area
MP 08_0252

Sam McGuiness
'Willowmere'
Boorowa
NSW 2586

19thDecember

The Director General
Major Development Assessment
Department of Planning and Infrastructure
GPO Box 39
SYDNEY NSW 2001

Dear Sir

Re: Proposed Flyers Creek wind Farm Blayney Local Government Area
Application reference: MP 08_0252

It is incomprehensible to most decent people that the current NSW Government
would allow wind turbine developments, that force people to live in such
turbulence as in these following documents, to be approved.

This against public policy and will result in legal challenges, and for those whom
do not understand the legal system, civil disobedience would be their only
option.

We believe this development is totally inappropriate given its close proximity to
where people live and work.

Yours faithfully

Sam McGuiness

CHANGING LOCAL ENVIRONMENT

This is a photo showing turbines in the ocean and the vapour trail caused by their turbulence

Turbulence and inversions of the near surface air are occurring as the turbines spin.

Wind turbines do alter the local environment.

Bureau of Meteorology has windfarm anomalies showing on radar!!!!!

Department of Atmospheric Sciences, University of Illinois, 209 S. Gregory St., Urbana, IL 61801, USA

The typical length-scale of the wind farm wakes is approximately 20 km that is independent of the size of the wind farms as well as background meteorology.

While the strongest impacts occur within the wind farms, they can also be felt up to a significant distance beyond the confines of the wind farms, especially in the downwind direction.

Impacts from wind turbines on surface meteorological conditions are likely to affect agricultural practices as well as communities living in residential areas around the farms.

The above photo graphically shows, living and working near turbines is causing huge problems.
Poor planning, rushed developments in inappropriate areas.

The molestation of the natural air flow can extend 20 km beyond the turbines.!??

Simulating impacts of wind farms on local hydrometeorology

Somnath Baidya Roy*

Department of Atmospheric Sciences, University of Illinois, 209 S. Gregory St., Urbana, IL 61801, USA

ARTICLE INFO

ABSTRACT

Wind power is one of the fastest growing energy sources in the world, most of the growth being in large wind farms that are often located on agricultural land near residential communities. This study explores the possible impacts of such wind farms on local hydrometeorology using a mesoscale model equipped with a rotor parameterization based on data from a commercial wind turbine. Results show that wind farms significantly affect near-surface air temperature and humidity as well as surface sensible and latent heat fluxes. The signs of the impacts, i.e., increase or decrease, depend on the static stability and total water mixing ratio lapse rates of the atmosphere. The magnitudes of these impacts are not only constrained by the hub-height wind speed but also depend to some extent on the size of the wind farms. Wind farms also affect the hydrometeorology of an area up to 18–23 km downwind. More work is required to conclusively estimate the length-scale of wind farm wakes. This study is one of the first few to provide realistic estimates of possible impacts of wind farms. The model developed and used in this study can help in assessing and addressing the environmental impacts of wind farms thereby ensuring the long-term sustainability of wind power.

1. Introduction

Studies with global and regional climate models have shown that extremely large wind farms may have strong impacts on weather and climate at local, regional and global scales (Baidya Roy et al., 2004; Keith et al., 2004; Adams and Keith, 2007; Kirk-Davidoff and Keith, 2008; Barrie and Kirk-Davidoff, 2010; Wang and Prinn, 2010). A recent study by Baidya Roy and Traiteur (2010) was the first to provide observational evidence of meteorological impacts of wind farms. The observations were taken at 2 towers, one upwind and another downwind of the wind farm. Additionally, that study showed that the impacts are caused by enhanced vertical mixing due to turbulence in the wake of wind turbine rotors.

Existing studies have used 2 different approaches to incorporate wind farms in atmospheric models. In both of these approaches wind farms are parameterized as subgrid-scale features. This is unavoidable because the horizontal spatial resolution of atmospheric models is too coarse to resolve wind turbines and wind farms. Studies with global climate models (Keith et al., 2004; Adams and Keith, 2007; Kirk-Davidoff and Keith, 2008; Barrie and Kirk-Davidoff, 2010; Wang and Prinn, 2010) have used a roughness-length approach where wind farms are represented by grid cells with high roughness lengths. The major challenge in

this approach is to find values of roughness length appropriate for wind farms. In contrast, Baidya Roy et al. (2004) and Baidya Roy and Traiteur (2010) have parameterized individual rotors as elevated sinks of momentum and sources of turbulent kinetic energy (TKE). Their rotor parameterization is intuitive but very idealized because it assumes a constant coefficient of performance (C_p) that is likely to produce unrealistic estimates of the impacts of wind farms.

The current study improves upon the Baidya Roy and Traiteur (2010) study by using a realistic rotor parameterization based on data from a late-model commercial turbine. Using a regional climate model equipped with a state-of-the-art microphysics and land-surface scheme this study also looks at the impacts of wind farms on near-surface temperature, humidity and surface fluxes of sensible and latent heat. This effort is in contrast with Baidya Roy and Traiteur (2010) that exclusively focused on air temperature. Additionally this study also examines the spatial distribution of the impacts within and downwind of the wind farms especially focusing on the importance of the spatial scale of wind farms.

Wind and other renewable energy sources are likely to be a part of the solution of the atmospheric carbon and climate change problem (Pacala and Socolow, 2004). Hence, wind power features prominently in the future energy plans of all industrial economies (Global Wind, 2008). It is currently one of the fastest growing energy sources in the world and will continue to do so in the near future. Most of the growth is in the utility sector (Wiser et al., 2007) consisting of large turbines and farms that are continuously increasing in power generation capability and spatial scale.

* Tel.: +1 2172441123.
E-mail address: sbroy@atmos.uiuc.edu

This study will improve our understanding of how these mega-structures interact with atmospheric boundary layer (ABL) dynamics and thermodynamics and provide realistic quantitative estimates of the possible impacts of wind farms on local hydrometeorology. The findings of this study will play a critical role in developing strategies to address these impacts thereby ensuring the long-term sustainability of wind power.

2. Impacts of wind farms on surface hydrometeorology

2.1. Model description and configuration

The Regional Atmospheric Modeling System or RAMS (Cotton et al., 2003; Pielke et al., 1992) was used to conduct a set of 306 simulations to investigate the impact of wind farms on local hydrometeorology. RAMS solves the full three-dimensional, compressible, nonhydrostatic dynamic equations, a thermodynamic equation and a set of microphysics equations. The system was closed with the Mellor-Yamada level 2.5 scheme (Mellor and Yamada, 1977) that explicitly solves for TKE while parameterizing other second-order moments. The coordinate system was rectangular Cartesian in the horizontal and terrain-following σ-type (Clark, 1977) in the vertical. The lateral atmospheric boundary conditions were zero-gradient inflow-outflow type following Klemp and Wilhelmson (1978). The bottom boundary conditions were supplied by LEAF3, the Land Ecosystem–Atmosphere Feedback model (Walko et al., 2000) version 3, dynamically coupled with RAMS. Radiative transfer within the atmosphere was simulated with a 2-stream scheme (Harrington, 1997) that treats the interaction of 3 solar and 5 infrared bands with atmospheric gases and hydrometeors. A detailed bulk microphysics scheme (Walko et al., 1995; Meyers et al., 1997) was used to prognose mixing ratio and number concentration of 7 different species of moisture and interactions between them in the atmosphere.

RAMS was used to simulate a rectangular domain, 107 km in the zonal (west–east) direction and 23 km in the meridional (south–north) direction, discretized in the horizontal with 1 km spacing (Fig. 1). The zonal alignment of the rectangular domain as well as the wind farm provides distinct computational advantages that are discussed later in this section. The vertical grid consisted of 19 layers of varying thickness. The heights of the atmospheric levels are shown in Table 1. With 9 layers in the lowest 1 km, this vertical grid can adequately resolve small-scale turbulent processes in the ABL. For simplicity, the domain was assumed to be a flat terrain at sea-level covered with bare soil.

The simulated wind farm was designed to be approximate a 7 × 3 array of the Gamesa G80-2.0 MW wind turbines (Gamesa 2010) spaced 1 km apart. According to the specifications, each G80-2.0 MW turbine is 100 m tall with 40 m rotor blades (80 m rotor diameter).

The 1-km spacing (12.5 rotor diameter) used in this study is slightly larger but not unrealistic compared to current recommended standards (Denholm et al., 2009). The wind farm was represented by introducing a rotor parameterization in the third atmospheric layer of a 7 × 3 array of grid cells in the center of the domain. The rotors were represented by a subgrid parameterization that assumes a rotor to be an elevated sink of momentum and a source of TKE. The rotor parameterization was implemented as follows:

- The turbines occupied 21 grid cells in the center of the model domain with a rotor located in the third atmospheric layer of each grid column. This layer is 80 m thick and located at a height of 100 m. Thus, the rotors can be completely contained within these grid cells.
- At each model timestep, the volume of air passing through the rotor is $\Delta V = \pi R^2 |\vec{U}| \Delta t$, where R=length of rotor blade, $\vec{U}$=wind velocity in the third atmospheric layer (wind turbine hub-height), and Δt=model timestep.
- The mass of the said volume of air is $\Delta M = \rho \Delta V$ where ρ is the density of air.
- The resolved kinetic energy (RKE) of the air passing through the rotor: $\Delta E = 1/2\Delta M |\vec{U}|^2$.
- If $4\,\mathrm{m\,s^{-1}} < |\vec{U}| < 25\,\mathrm{m\,s^{-1}}$, then δE energy is removed from the atmospheric flow for generating power. The value of δE is calculated by simple linear interpolation from the power curve data of the Gamesa G80–2.0 MW turbine (Gamesa, 2010).

Table 1
Heights of the RAMS model atmospheric levels.

Model level	Height (m)
1	0
2	30
3	60
4	140
5	240
6	350
7	470
8	614
9	786
10	994
11	1242
12	1541
13	1899
14	2329
15	2845
16	3465
17	4208
18	5099
19	6169
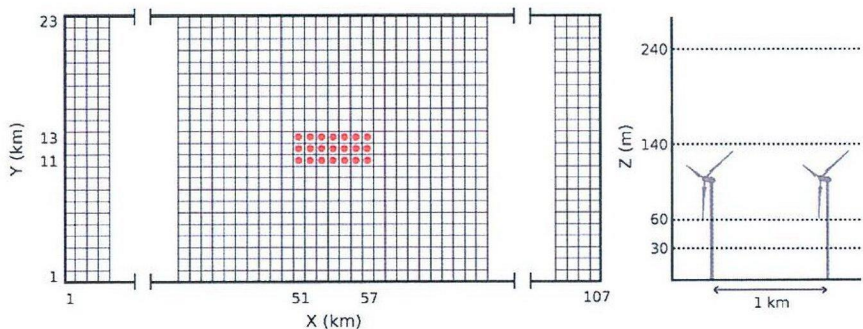
Fig. 1. Schematic diagram of (left) horizontal grid structure with the grid cells containing the rotors marked by the red circles in the middle and (right) vertical grid structure showing the lowest 4 atmospheric layers.
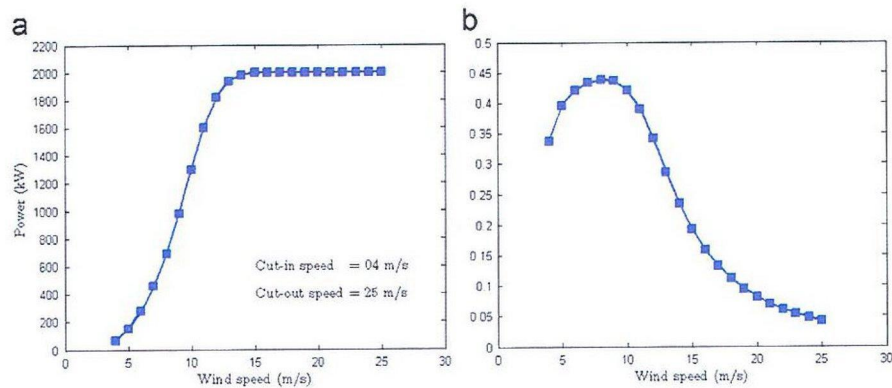
Fig. 2. (a) Power curve and (b) coefficient of performance of the Gamesa G80-2.0 MW turbine as a function of hub-height wind speed. Calculations were made assuming air density = 1.225 kg/m^3.

The fraction of energy passing through the rotor that is captured for power generation by turbines is known as the coefficient of performance (C_p). C_p is a function of wind speed and rotor design, reaching a maximum of 16/27, known as the Betz Limit (Frandsen, 1992). Fig. 2 shows that the C_p of the Gamesa G80-2.0 MW turbine reaches a maximum of about 0.45 at 10 m/s wind speeds but falls rapidly to less than 0.05 at high wind speeds. It is important to note that the power curve of a wind turbine refers to electrical power. The aerodynamic power absorbed by the turbine is larger by about 10% accounting for gearbox and generator losses (Hau, 2005).

- Observations from the San Gorgonio wind farm show that the TKE of the air passing through the rotor is approximately 5 m^2 s^{-2} higher than the ambient value and remains fairly constant with varying wind speeds (Baidya Roy et al., 2004). Similar values have been reported by Taylor (1983). Thus, TKE generated in the entire wake due to turning of the rotor can be represented by $\Delta e = 5\rho \Delta V$.

- The TKE of the grid cell can now be calculated as $e_1 = e_0 + \Delta e / \rho V$, where e_0 and e_1 are the TKEs of the grid cell before and after the rotor parameterization subroutine is called, respectively, and V is the volume of the grid cell.

- The RKE of the grid cell containing the rotor decreases because δE part of it is removed to generate electricity while Δe part is converted to turbulence in the wake. So, at the end of the timestep, the RKE of the grid cell becomes $E_1 = E_0 - \delta E - \Delta e / \rho V$, where E_0 and E_1 are the RKEs of the grid cell before and after the rotor parameterization subroutine is called, respectively.

- The wind velocity of the cell can now be calculated as $\vec{U} = \sqrt{2E_1 / \rho V}$.

In the Mellor-Yamada (1977) closure scheme, TKE and momentum are prognosed. The rotor parameterization effectively adds a source term to the TKE equation and a sink term to the momentum equation. . The magnitude of the source/sink terms is calculated at every timestep with respect to the volume of air passing through the rotor (ΔV) but the source/sink terms are applied to the entire grid cell volume (V). It is important to note that ΔV is many orders of magnitude smaller than V. For example at a wind speed of 10 m/s, $\Delta V = 100,528$ m^2 but $V = 80,000,000$ m^2 and hence, ΔV is only 0.125% of V. So, when the source/sink terms are averaged over the entire grid cell at a particular timestep, they do not produce an instantaneous shock large enough to destabilize the system. However, the cumulative impact of the source/sink terms can be large if the wind speeds are sustained within the operating range of the wind turbine. The momentum deficit and TKE enhancement in the wake grows with time and alters the

Table 2
Sounding data from the following WMO stations were used to initialize the RAMS model simulations.

Station	Latitude, Longitude
Albuquerque, NM	35/02N, 106/37W
Boise, ID	43/34N, 116/13W
Denver Int. Airport, CO	39/46N, 104/52W
Desert Rock, NV	36/37N, 116/01W
Elko, NV	40/52N, 115/44W
Flagstaff, AZ	35/14N, 111/49W
Glasgow, MT	48/13N, 106/37W
Grand Junction, CO	39/07N, 108/32W
Great Falls, MT	47/27N, 111/23W
Medford, OR	42/23N, 122/53W
Oakland, CA	37/45N, 122/13W
Quillayute, WA	47/47N, 124/33W
Reno, NV	39/34N, 119/48W
Riverton, WY	43/04N, 108/29W
Salem, OR	44/55N, 123/01W
Salt Lake City, UT	40/47N, 111/57W
San Diego, CA	32/50N, 117/07W
Santa Teresa, NM	31/52N, 106/42W
Spokane, WA	47/38N, 117/32W
Tucson, AZ	32/07N, 110/56W
Vandenberg AFB, CA	34/44N, 120/33W

mean momentum and TKE of the entire grid cell, thereby significantly affecting the vertical transport of heat and moisture.

The simulations were initialized with atmospheric sounding data for November 1, 2008, February 1, May 1 and August 1, 2009, from 21 World Meteorological Organization (WMO) stations in western US (Table 2). These observations are taken by radiosondes that are small automated disposable sensors attached to weather balloons. These sensors sample the air every 5 s while the balloon is ascending and transmit the data to ground-based data acquisition and processing centers. Depending on the speed of ascent, the vertical spatial resolution of the data is in the 10–100 m range in the troposphere. The sensors record a wide array of atmospheric dynamic and thermodynamic properties of which pressure, temperature, relative humidity, wind speed and wind direction were used for model initialization. Only the wind directions in the input soundings were changed to 270° so that all wind was assumed to be westerly, i.e. blowing from west to east. This assumption, in conjunction with the zonal (west–east) orientation of the model domain and the simulated wind farm optimizes computational costs against experimental requirements. In this configuration, the wind farm is 50 km away from both the inflow (western) and outflow (eastern) boundaries. Thus perturbations from the inflow boundary are less likely to affect the wind farm and the wind farm wake is less likely to affect the

outflow boundary. The meridional (south–north) transport of perturbations is mainly by diffusion due to the absence of meridional wind. This is a slow process and hence the wind farm can be placed closer to the domain boundaries. This allows for a rectangular 107 km × 23 km computational domain, as opposed to a square 107 km × 107 km domain thereby saving a considerable amount of computing resources.

The input soundings were available for 0Z and 12Z, corresponding to 4 or 5 am (0Z) and 4 or 5 pm (12Z) local standard time, depending on whether the stations were in the US Mountain or Western Standard time zones. In total, 153 complete soundings were available covering the entire annual cycle. The model was integrated for 1 h with a timestep of 2 s. For each initial condition, a pair of simulations was conducted: one with the rotor parameterization switched off (control) and another with the parameterization turned on (wind farm case).

2.2. Results

A comparison of each pair of wind farm and control simulations was conducted to study the effect of wind farms on near-surface temperature, humidity and surface sensible and latent heat fluxes as a function of ambient atmospheric flow parameters. In the context of the RAMS model simulations, near-surface refers to the lowest model level centered at a height of 15 m above the ground surface. For each simulation, the 4 variables were averaged in space over the 21 points corresponding to the wind farm location as well as in time over the entire simulation period. The impact of wind farms was then quantified by calculating the differences in these 4 space-time averaged variables between *each pair* of control and wind farm simulations. Ambient lapse rate and hub-height wind speed were calculated from each

control simulation by averaging over the 21 points corresponding to the location of the wind farms. Only the lapse rate in the lowest 350 m layer was considered because this layer is likely to be the most affected due to the turbulent rotor wakes. The 0–350 m lapse rate was calculated as the equivalent potential temperature (θ_e) gradient between the 1st and the 5th atmospheric levels.

Baidya Roy et al. (2004) and Baidya Roy and Traiteur (2010) found that the impacts at the surface are due to the enhanced vertical mixing generated by the turbulence in the wakes of the spinning rotors. Consider a statically stable environment where temperature increases with height. Turbulence will mix warm air down and cool air up leading to a warming at the surface and a cooling aloft. The opposite will occur when the atmosphere is statically unstable. This phenomenon is clearly evident in Fig. 3a where we see a general increase in surface temperatures under positive lapse rates and a decrease under negative lapse rates. This result is qualitatively similar to Baidya Roy and Traiteur (2010) but a quantitative comparison is not appropriate because the simulations in the present study are significantly different due to inclusion of moisture effects. In this figure, θ_e is used instead of actual temperature as a measure of environmental stability. Equivalent potential temperature of an air parcel is defined as the temperature a parcel of air would have if it is transported adiabatically from its current altitude at pressure p to the standard pressure level p_0 and all the water vapor in the parcel condenses, releasing its latent heat. Mathematically, θ_e is given by

$$\theta_e \approx \left(T + \frac{L_v}{C_p}r\right)\left(\frac{p_0}{p}\right)^{R_d/C_p}$$

where T is the temperature of the parcel at pressure p, r is the mixing ratio, p_0 is the standard reference pressure equal to 100 kPa, L_v is the latent heat of vaporization, C_p is the specific
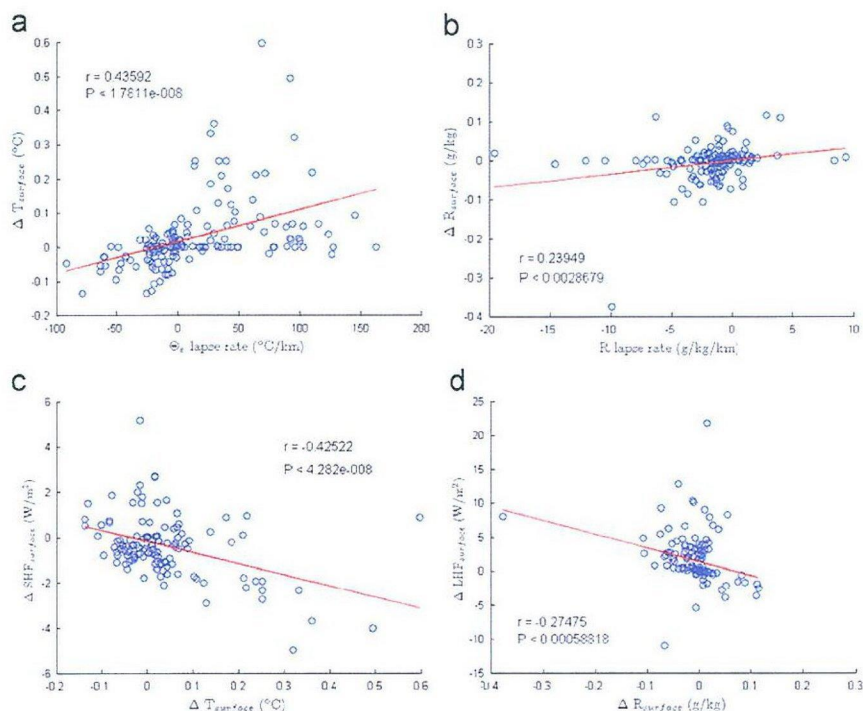
Fig. 3. Scatter plot showing the relationship between (a) the change in near-surface air temperature and the ambient 0–350 m equivalent potential temperature lapse rate; (b) the change in near surface total water mixing ratio and the ambient 0–350 m total water mixing ratio lapse rate; (c) the change in surface sensible heat flux and the change in near-surface air temperature; and (d) the change in surface latent heat flux and the change in near surface total water mixing ratio. The scatter plots consist of 153 points, each of which represents the difference between the control and wind farm simulation for a particular initial condition. These differences are averaged over the 21 points corresponding to the location of the wind farm and the 1-h simulation period. Statistical significance of the correlation coefficient was estimated using the Student's *t*-test.

heat of dry air at constant pressure and R_d is the specific gas constant for air. θ_e is conserved during moist adiabatic transport. Since almost all atmospheric transport is moist adiabatic, θ_e lapse rate is the most appropriate measure of atmospheric stability (Wallace and Hobbs, 2006). Thus, the change in surface air temperature (ΔT) exhibits a statistically significant positive correlation with θ_e lapse rate.

The same phenomenon can be observed in Fig. 3b showing the relationship between change in surface total water mixing ratio (R) and the ambient mixing ratio lapse rate. Total water mixing ratio, defined as the amount of moisture present in each kg of dry air, is a measure of water content of an air parcel. If the R lapse rate is positive, i.e., humidity increases with height, turbulence mixes relatively moist air down and relatively dry air up, leading to a net moistening of near-surface air and vice versa. Thus, the change in surface humidity (ΔR) shows a statistically significant positive correlation with respect to R lapse rate.

Change in near-surface air temperature and humidity has a strong impact on the fluxes of sensible and latent heat between the ground and the atmosphere. Surface sensible heat flux (SHF) is a function of the gradient between the ground and the near-surface air temperatures. Consider a typical late afternoon (4 pm) scenario when the temperature has a negative lapse rate and the ground is warmer than the air above it. Hence, the surface sensible heat flux is positive, i.e., heat is transported from the ground to the atmosphere. Under this condition, wind farms produce a cooling effect on the near-surface air temperatures, thereby increasing the ground-air temperature gradient. Consequently, more heat is transported from the ground to the atmosphere, i.e., the surface sensible heat flux increases. On the other hand, during early mornings (4 am), the lapse rate is typically positive and the surface sensible heat flux is negative because the air is warmer than the ground. As described earlier, wind farms lead to a warming of the surface air, making both the ground-air temperature gradient and the surface sensible heat flux more negative. Thus a positive ΔT near the surface leads to a negative ΔSHF and vice versa. This phenomenon is demonstrated in Fig. 3c where ΔT and ΔSHF exhibit a statistically significant negative correlation. By similar logic, near-surface ΔR and surface latent heat flux (LHF) are negatively correlated as well (Fig. 3d). LHF is driven by ground-air moisture gradient. Thus, LHF increases due to a drying of the near-surface air and decreases due to an increase in near-surface R values.
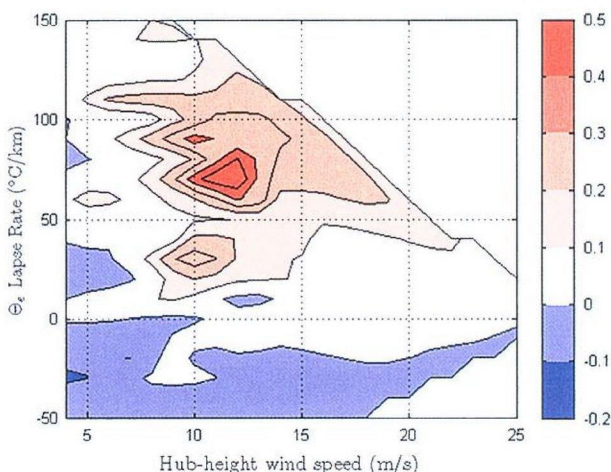

Fig. 4. Change in near-surface air temperature (°C) averaged over the entire wind farm plotted as a function of ambient 0–350 m equivalent potential temperature lapse rate (°C/km) and turbine hub-height wind speed (m/s).

Fig. 4 shows that ΔT is a function of both θ_e lapse rate and the turbine hub-height (100 m) wind speed. Maximum impacts occur at intermediate wind speeds (10–13 m/s) and intermediate positive lapse rates ($\sim$70 °C/km). The values of ΔT are small at very high as well as very low wind speeds. Typically high wind speeds are associated with neutral stability where θ_e lapse rate is very small. Under this condition, the atmosphere is already well-mixed and hence extra mixing by wake turbulence has little to no impact on near-surface air temperatures. At very weak wind speeds, even though the lapse rates can be very high, the impacts are small. This is because the rotors probably function intermittently as the wind speeds frequently drop below the cut-in speed of the Gamesa G80-2.0 MW turbine.

3. Effect of wind farm size

The previous analysis deals with the mean hydrometeorological impacts within a small wind farm. A series of sensitivity studies were conducted to explore 2 additional questions:

i. Does the magnitude of the impacts depend on the spatial scale of the wind farms?
ii. What is the spatial distribution of these effects within and downwind of wind farms?

In these simulations, the same model configuration as before was used. The model domain was extended to 125 km to accommodate downwind wind farm wakes. Apart from a control case, a total of 5 other simulations were conducted with wind farms of length $\lambda = 5, 10, 15, 20$ and 25 km where the wind farms started from the 51st grid point of the domain and extended up to the 55th, 60th, 65th, 70th and 75th grid points in the zonal (west–east) directions, respectively. They all spanned 3 grid points in the meridional (south–north) direction.

The simulations were initialized with sounding data collected on 12Z (5 am LST) August 1, 2009, from the Glasgow, Montana, NWS station. This particular dataset was used because in the previous simulation, this sounding produced the strongest impact on near-surface air temperature. The same experiments were repeated with data collected on 12Z (4 am LST) November 1, 2008 from the NWS station in Quillayute, Washington. Both cases had similar stability with positive θ_e lapse rates of similar magnitude. However, the mean hub-height wind speed at the Glasgow station (11.4 m/s) was almost double that of the Quillayute station (6.1 m/s). Additionally, the mixing ratio lapse rate was positive at Glasgow but negative at Quillayute. The results of this sensitivity study are plotted in Fig. 5 (Glasgow) and 6 (Quillayute) and match quite well with the results of the experiments discussed in the previous section. All simulations at the Glasgow station produced increased surface temperature and humidity and reduced surface sensible and latent heat flux. The Quillayute station produced a warming and drying leading to lower sensible heat flux but higher latent heat flux (Fig. 6).

The figures show that the magnitude of the impacts depends on the scale of the wind farm. In the Glasgow case, the peak magnitude increases as λ increases from 5 to 15 km but subsequently remains constant at the 15 km level for longer wind farms. For wind farms with $\lambda \leq 15$ km, the impacts increase with downwind distance from the western edge of the farms till reaching the peak at the end of the wind farms and start decreasing thereafter. For larger wind farms, the peak occurs 15 km into the wind farms, stays more or less constant at that level till the end is reached and then starts to decrease. In the Quillayute case, the peak magnitude is reached inside the 10 km wind farm. The peak impact remains approximately at that level
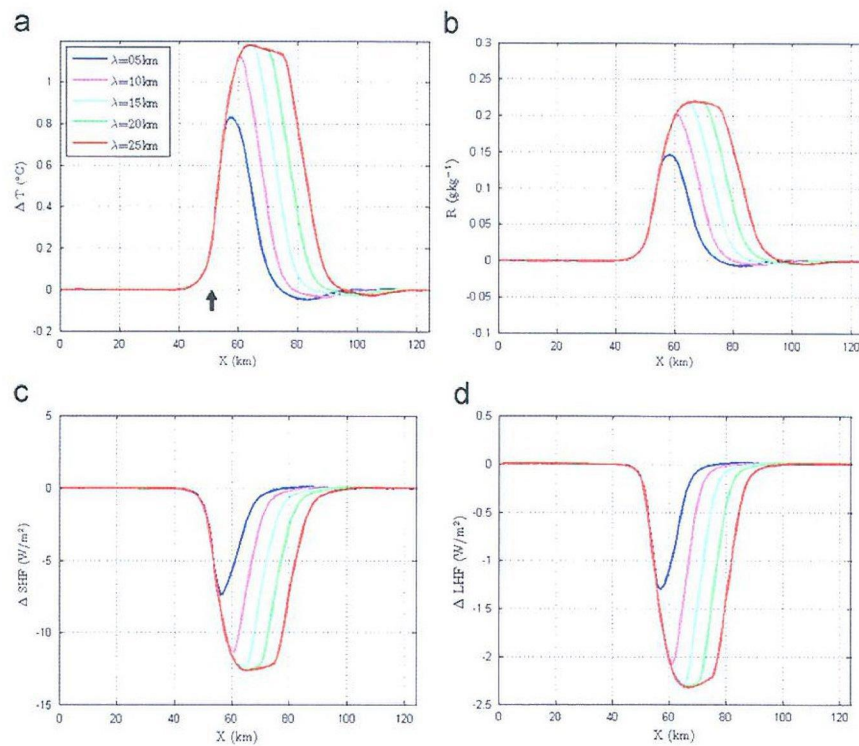
Fig. 5. Meridionally averaged changes in (a) near-surface air temperature, (b) near-surface total water mixing ratio, (c) surface sensible heat flux and (d) surface latent heat flux over wind farms of different sizes using initial conditions from 12Z August 1, 2009, from Glasgow, MT. The black arrow marks the western edge of the wind farms.
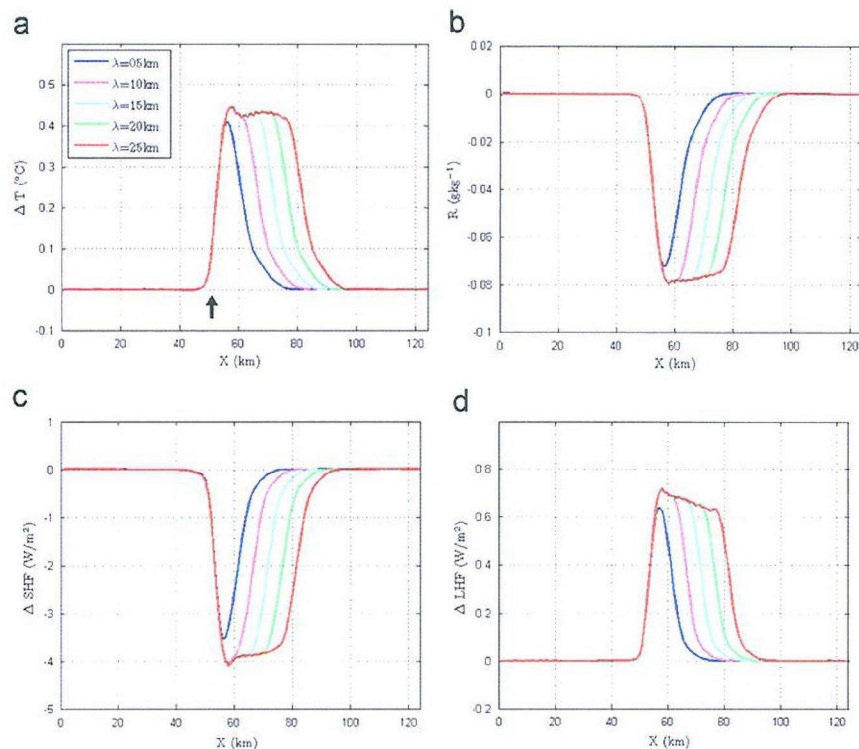

Fig. 6. Same as in Fig. 5 but with initial condition from Quillayute, WA, on 12Z November 1, 2008.

and location for larger wind farms. This pattern implies that the magnitude and location of the peak impacts is constrained by the kinetic energy of the flow, i.e., the turbine hub-height wind speed.

For small wind farms, the peak and its downwind location increase with wind farm size. Once the constraint set by the flow is reached, the peak and its location do not change however large

the wind farm may be. This pattern is evident for all 4 hydro-meteorological parameters in both locations.

While the strongest impacts occur within the wind farms, they can also be felt up to a significant distance beyond the confines of the wind farms, especially in the downwind direction. For wind farms of all size, the impacts start to decrease right at the eastern edge gradually becoming zero at a distance of 18–23 km from the edge. It appears from these simulations that the length-scale of wind farm wakes is approximately 20 km irrespective of the length-scale of the wind farms and background meteorological conditions.

4. Discussions

One of the major strengths of this work is the integration of real-world data in the rotor parameterization as well as the initial conditions to ensure that the experimental results are realistic. A typical numerical sensitivity study would have involved experimenting with different initial conditions such as keeping the lapse rate constant and linearly varying the wind speeds or using a range of lapse rates for a constant wind speed. Such studies can provide useful insights into how background meteorology affects the interactions between wind farms and atmospheric flow. However, many of these idealized experiments are likely to generate unrealistic scenarios like high wind speeds in unstable environments. By using real meteorological observations, this work produced results that are likely to be realistically observed in operational wind farms.

This study uses RAMS, a well-known mesoscale atmospheric model with the capability to simulate the interactions between wind farms and the atmospheric boundary layer. A subgrid-scale rotor parameterization is developed and implemented in RAMS to conduct numerical experiments. Subgrid parameterizations are the only way to represent rotors in mesoscale and coarser atmospheric models because wind turbine rotors and wakes are many orders of magnitude smaller than atmospheric mesoscale flow (Brand, 2007). A major advantage of RAMS and some other mesoscale models is the availability of 1.5 order closure scheme where momentum vectors and TKE are prognosed while other second-order moments representing turbulent fluxes are parameterized. The 1.5 order closure scheme allows for the implementation of the momentum sink/TKE source parameterization for wind turbine rotors. In contrast most climate models use a 1st order closure with no prognostic equation for TKE. Hence, studies using climate models have represented wind farms as surface roughness elements (Keith et al., 2004; Kirk-Davidoff and Keith, 2008; Barrie and Kirk-Davidoff, 2010; Wang and Prinn, 2010).

A wide range of studies have developed wind turbine wake models (Vermeer et al., 2003; Brand, 2007; Calaf et al., 2010). Most of these models operate at very high spatial resolution that can resolve the wakes. Some of the computational fluid dynamics models can even resolve individual rotor blades. Some of them use a 2nd order closure capable of prognosing turbulent transport. These models can resolve the 3-dimensional spatial structure of turbine wakes. However, these models are computationally too expensive to conduct a large ensemble of simulations to study the impacts of wind turbines on atmospheric flow under a wide range of initial and boundary conditions. Most importantly, the existing wake models focus entirely on the dynamics of atmospheric flow. In order to study the impact of wind farms on local hydrometeorology a model that also represents atmospheric thermodynamics and heat and moisture fluxes within and across model boundaries is required. Hence, there is a need for developing high-resolution models capable of simulating the aerodynamic and thermodynamic properties of wind turbine wakes.

These models will have to be calibrated with data from field campaigns and wind tunnels capable of incorporating non-neutral thermal stratification. It would be interesting to see if outputs from these high-resolution models, when averaged over appropriate spatial scales, can match the results from mesoscale and climate models.

Two aspects of the rotor parameterization used here needs to be explored further. First, the turbine power curve quite likely underestimates the momentum sink term. The power curve gives the electrical power output from the turbine as a function of wind speed. The aerodynamic power loss from the atmospheric flow is larger than the electrical power generated because some of the power is lost by generators and gearboxes. Field or laboratory observations are required to accurately estimate the aerodynamic power loss as a function of wind speed. Alternatively, sensitivity studies can be conducted to estimate the uncertainties generated by inaccuracies in the momentum sink term. Second, a constant TKE source is used in this work. Observations from San Gorgonio show that increase in TKE in the wind farm wake changes little with wind speed. However, this phenomenon may be unique to the location and period of the field campaign.

Even though this work uses 153 different sounding profiles, it is not an exhaustive set by any means. Other types of meteorological situations are certainly possible. One particular phenomenon of interest to wind energy companies is the low-level jet (LLJ, Stull, 1993). It is a low-altitude band of very high speed wind overlying a stable ABL such as the Great Plains nocturnal jet in the US and the Somali Jet in East Africa. There was no evidence of jets in the sounding data. It is possible that the lengthscales of wind farm wakes may exhibit a dependence on wind speeds in the presence of very strong winds. Hence there is a need for continuing this investigation with other kinds of initial conditions.

Another issue that demands a follow-up investigation is the question of time-scale. This study considers processes with time-scales of 1 h or less. Over longer timescales the response of the land surface and consequently, the effects on near-surface air temperature and humidity may be significantly different. To study these processes, the model needs to be driven by appropriate boundary conditions reflecting large-scale weather systems passing through the simulation domain.

5. Conclusions

This study uses a regional climate model to explore the possible impacts of wind farms on local hydrometeorology. A subgrid-scale rotor parameterization based on data from a commercial wind turbine was developed and implemented in the model for this study. Numerical experiments show that wind farms generate statistically significant impacts on near-surface air temperature and humidity as well as surface sensible and latent heat fluxes. These impacts depend on the atmospheric lapse rates of equivalent potential temperature and total water mixing ratio. Sensitivity studies show that these impacts are not confined to the wind farms but extend a significant distance downwind. The typical length-scale of the wind farm wakes is approximately 20 km that is independent of the size of the wind farms as well as background meteorology. However, more simulations with a wider range of initial conditions are required to conclusively demonstrate this phenomenon.

This study has significant implications for future energy and land use policy. Data show that wind power is on the verge of an explosive growth, especially in the US with many wind farms are coming up over agricultural lands. Impacts from wind turbines on surface meteorological conditions are likely to affect agricultural practices as well as communities living in residential areas

around the farms. Current research on impacts of wind farms on weather and climate primarily looks at global-scale impacts from extremely large wind farms. This study is one of the first few to provide realistic estimates of possible impacts of wind farms. The model developed and used in this study can help in assessing and addressing the environmental impacts of wind farms thereby ensuring the long-term sustainability of wind power.

References

Adams, A.S., Keith, D.W., 2007. Wind energy and climate: modeling the atmospheric impacts of wind energy turbines. EOS Trans., 2007. AGU 88.

Baidya Roy, S., Pacala, S.W., Walko, R.L., 2004. Can large wind farms affect local meteorology? J. Geophys. Res., 109. doi:10.1029/2004JD004763.

Baidya Roy, S.B., Traiteur, J.J., 2010. Impact of wind farms on surface air temperatures. Proc. Natl. Acad. Sci.. doi:10.1073/pnas.1000493107.

Barrie, D., Kirk-Davidoff, D.B., 2010. Weather response to a large wind turbine array. Atmos. Chem. Phys. 10, 769–775.

Brand, A.J., 2007. Modeling the effect of wind farming on mesoscale flow Part1: flow model. J. Phys. Conf. Ser. 75, 012043.

Calaf, M., et al., 2010. Large-eddy simulation study of fully developed wind-turbine array boundary layers. Phys. Fluids 22 (015110), 2010. doi:10.1063/1.3291077.

Clark, T.L., 1977. A small-scale dynamic model using a terrain-following transformation. J. Comput. Phys. 24, 186–215.

Cotton, W.R., et al., 2003. RAMS 2001: current status and future directions. Meteorol. Atmos. Phys. 82, 5–29.

Denholm P., et al. 2009. Land-use requirements of modern wind power plants in the United States. Technical Report NREL/TP-6A2-45834, National Renewable Energy Laboratory, Boulder CO, 46 pp. Available online at ⟨http://www.nrel.gov/docs/fy09osti/45834.pdf⟩ accessed on 24/12/2010.

Frandsen, S., 1992. On the wind speed reduction in the center of large clusters of wind turbines. J. Wind Eng. Ind. Aerodyn. 39, 251–265.

Gamesa, 2010. Gamesa G80-2.0 MW. Available online at ⟨http://www.gamesa corp.com/files/File/G80-ingles.pdf⟩. Accessed on September 7, 2010.

Global Wind, 2008. Global Wind Energy Council, Brussels, Belgium, 2009.

Harrington, J.Y., 1997. The effects of radiative and microphysical processes on simulated warm and transition season Arctic stratus. Ph.D. thesis, Colorado State University, Fort Collins, CO.

Hau, E., 2005. Wind Turbines: Fundamentals, Technologies, Applications, Economics. Springer, Berlin 783 pp.

Keith, D.W., et al., 2004. The influence of large-scale wind power on global climate. Proc. Natl. Acad. Sci. 101, 16115–16120.

Klemp, J.B., Wilhelmson, R.B., 1978. The simulation of three-dimensional convective storm dynamics. J. Atmos. Sci. 35, 1070–1096.

Kirk-Davidoff, D.B., Keith, D.W., 2008. On the climate impact of surface roughness anomalies. J. Atmos. Sci. 65, 2215–2234.

Mellor, G.L., Yamada, T., 1977. Development of a turbulence closure model for geophysical fluid problems. Rev. Geophys. Space Phys. 20, 851–875.

Meyers, M.P., et al., 1997. New RAMS cloud microphysics parameterization, Part II: the two-moment scheme. Atmos. Res. 45, 3–39.

Pacala, S.W., Socolow, R., 2004. Stabilization wedges: solving the climate problem for the next 50 years with current technologies. Science 305, 968–972.

Pielke, R.A., et al., 1992. A comprehensive meteorological modeling system – RAMS. Meteorol. Atmos. Phys. 49, 69–91.

Stull, R.B., 1993. An Introduction to Boundary Layer Meteorology. Kluwer, Dordrecht, pp 520–526.

Taylor, G.L., 1983. Wake and performance measurements on the Lawson-Tancred 17 m horizontal-axis windmill. IEE Proc. 130, 604–612.

Vermeer, L.J., et al., 2003. Wind turbine wake aerodynamics. Prog. Aerospace Sci. 39, 467–510.

Walko, R.L., et al., 1995. New RAMS cloud microphysics parameterization, Part I: the single moment scheme. Atmos. Res. 38, 29–62.

Walko, R.L., et al., 2000. Coupled atmosphere-biophysics-hydrology model for environmental modeling. J. Appl. Meteorol. 39, 931–944.

Wallace, J.M., Hobbs, P.V., 2006. Atmospheric Science: An Introductory Survey. Academic, Burlington VT, pp 85–86.

Wang, C., Prinn, R.J., 2010. Potential climatic impacts and reliability of very large-scale wind farms. Atmos. Chem. Phys. 10 (2053–2061), 2010.

Wiser R., et al., 2007. Annual Report on US Wind Power Installation, Costs and Performance Trends: 2006, US Department of Energy, pp. 9–10.

Meteorological Explanation of Wake Clouds at Horns Rev Wind Farm

S. Emeis; Institute for Meteorology and Climate Research, Karlsruhe Institute of Technology
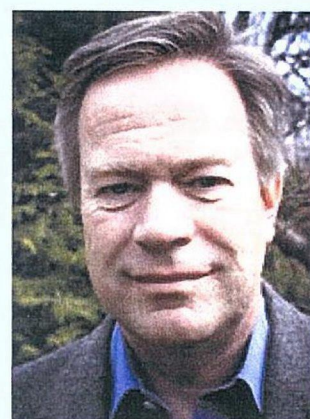
S. Emeis

ENGLISH

Abstract

The occurrence of wake clouds at Horns Rev wind farm is explained as mixing fog. Mixing fog forms when two nearly saturated air masses with different temperature are mixed. Due to the non-linearity of the dependence of the saturation water vapour pressure on temperature, the mixed air mass is over-saturated and condensation sets in. On the day in February 2008, when the wake clouds were observed at Horns Rev, cold and very humid air was advected from the nearby land over the warmer North Sea and led to the formation of a shallow layer with sea smoke or fog close above the sea surface. The turbines mixed a much deeper layer and thus provoked the formation of cloud trails in the wakes of the turbines.

Introduction

On February 12, 2008 wake clouds have been observed in the lee of the turbines at Horns Rev wind farm (Fig. 1). This seems to be a rare event since similar photos from other events are not known to the author. In the internet a few further photos can be found which show wind turbines in a deeper pre-existing fog layer, but no distinct wake clouds are visible in the lee of the turbines on those images (see e. g., http://www.dailymail.co.uk/news/article-1251721/Pictured-The-stunning-micro-climate-sea-fog-created-Britains-windfarms.html). The clouds which formed in the lee of the turbines at Horns Rev must be related to the wake turbulence produced by the wind turbines, because they spread exactly in the same way as wakes are supposed to do. Thus, the explanation must involve a condensation process which is fostered by turbulence.

Horns Rev is an offshore wind farm 14 to 20 km off the west coast of Jutland, Denmark, consisting of 80 wind turbines. These turbines are arranged in a regular rhomboidal array of 8 by 10 turbines. The eight rows of 10 turbines are oriented from West to East, the ten columns run from South-Southeast to North-Northwest (Fig. 2). Hub height is 70 m; rotor diameter is 80 m. Thus, the swept area is from 30 m to 110 m above the sea surface. The distance between the turbines is 560 m; the whole area of the wind farm is roughly 20 km². Together with information from a second image (not reproduced here) and the shadows visible in Fig. 1 it is quite clear that the view on Horns Rev wind farm is from the Southeast.

This paper will show that an explanation via the formation of mixing fog can be supported from the available mete-
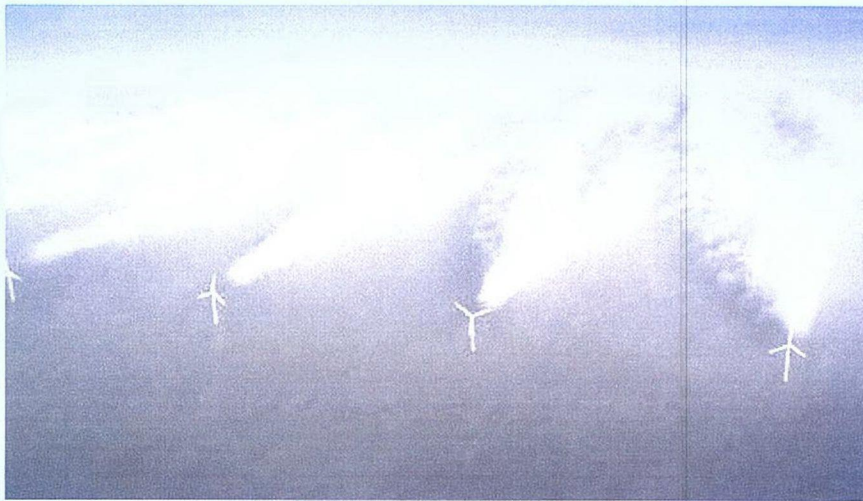
Fig. 1: Aerial view from the Southeast of wake clouds at Horns Rev on Februray 12, 2008
(© Vattenfall, Horns Rev 1 owned by Vattenfall. Photographer Christian Steiness)
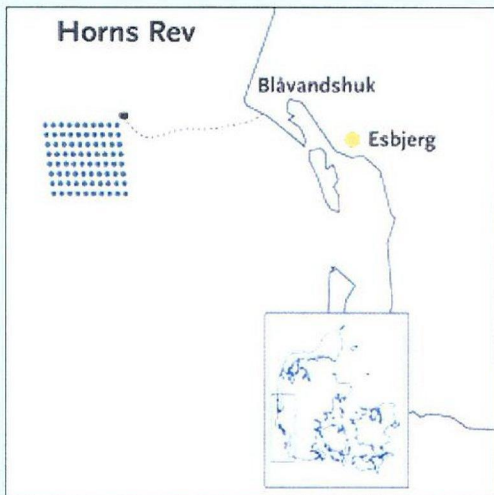
Fig. 2: Horns Rev wind farm
(from: http://www.hornsrev.dk/nyheder/brochurer/Horns_Rev_TY.pdf)

orological data for this event. After a short sketch of the theoretical basis of the formation of mixing fog and a characterization of the weather situation on that day, we will analyse the event depicted in Fig.1.

The Water Vapour Saturation Dependence on Temperature

The amount of water vapour which can exist in a given volume is limited. When the upper bound is reached the vapour is called saturated. The addition of further water vapour then leads to condensation and the formation of small droplets, if a sufficient number of condensation nuclei is available. The upper bound for water vapour content in a given volume is a function of temperature only. The temperature dependence of the saturation water vapour pressure E is described theoretically by the Clausius-Clapeyron equation involving the heat of condensation and the gas constant for water vapour. Approximately, the dependence of water vapour saturation pressure in hPa on temperature can be described more simply by Magnus' formula (Emeis 2000):

$$E(t) = 6.107 * 10^{a\, t/(b+t)}$$

Here t denotes air temperature in °C. a and b are two con-

stants (over water: $a=7.5$, $b=235$, over ice: $a=9.5$, $b=265.5$). As a rule of thumb the saturation water vapour pressure doubles every ten degrees between 0°C and 25°C. This means that the saturation water vapour curve in a (t, E)-diagram such as Fig. 3 is a steadily increasing upward-bended curve (full line in Fig. 3). This curve separates the under-saturated regime below the curve from the over-saturated regime above the curve. Water boils, if the saturation water vapour pressure reaches the ambient air pressure. This happens at 100°C if the ambient pressure is 1013.25 hPa.

Mixing of two saturated air masses of different temperature leads to a mixed air mass which is always oversaturated, because each straight line which connects two separate points on the saturation water vapour curve runs through the space above the curve between the two points. This is illustrated by the dashed line in Fig. 3.

Weather Situation on February 12, 2008

On February 12, 2008, when the formation of the wake clouds happened, Horns Rev was situated at the western flank of a large wintry high pressure system over the European continent in a weak southeasterly flow with roughly 5 m/s wind speed at 10 m height (Fig. 4). The radiosonde ascent on February

Fig. 3: Dependency of water vapour saturation pressure E (y-axis, in hPa) on air temperature t (x-axis, in °C) following Magnus' formula (full line) for the temperature range relevant for the present study. The straight dashed line connects the two state points (t=-1°C, rh=99 %) and (t=+5°C, rh=99 %) (rh: relative humidity). The interval between 0°C and 4°C where over-saturation occurs (the dashed line is above the full curve) is marked with vertical grey bars in Fig. 5.
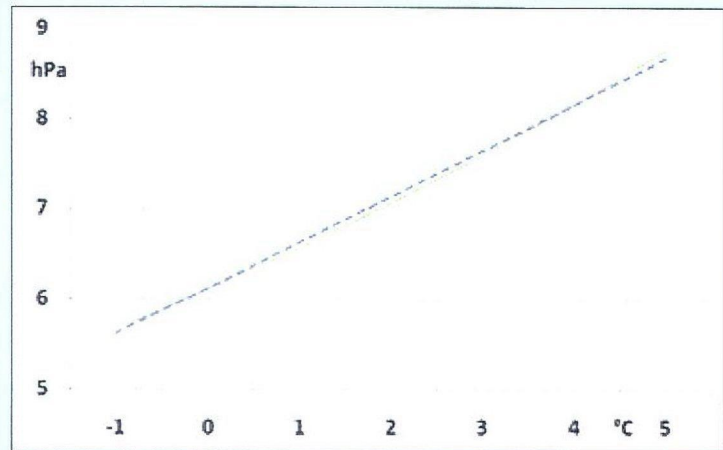

Fig. 4: Surface weather map for February 12, 2008 12 UTC showing 10 m winds in knots (full barb = 10 knots, halb barb = 5 knots) and surface pressure in hPa (thin grey lines).
© www.wetter3.de
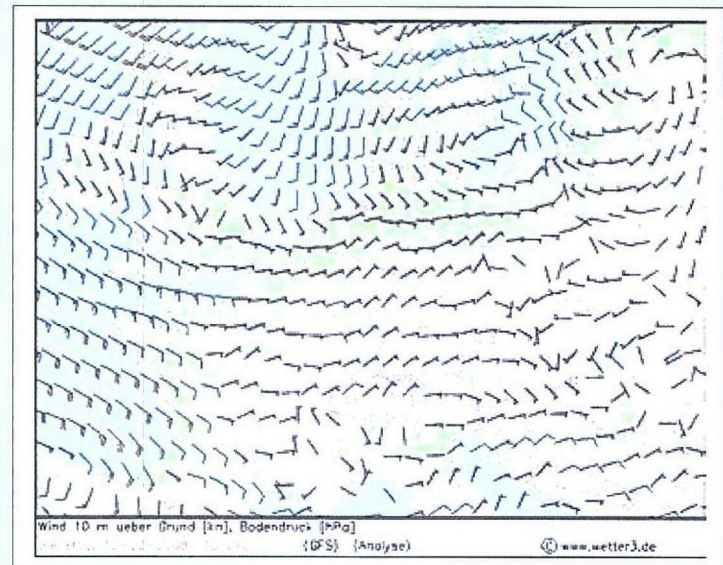
Fig. 5: Simplified sketch of vertical temperature profiles (full line) upstream (left) and downstream (right) of the wind turbines at Horns Rev during the formation of mixing fog. The vertical grey bars indicate the temperature range for which over-saturation and the formation of mixing fog can be expected (see Fig. 3); the dashed vertical lines indicate -1°C and +5°C. The large arrow indicates wind direction; the small bended arrows mark the wake turbulence.
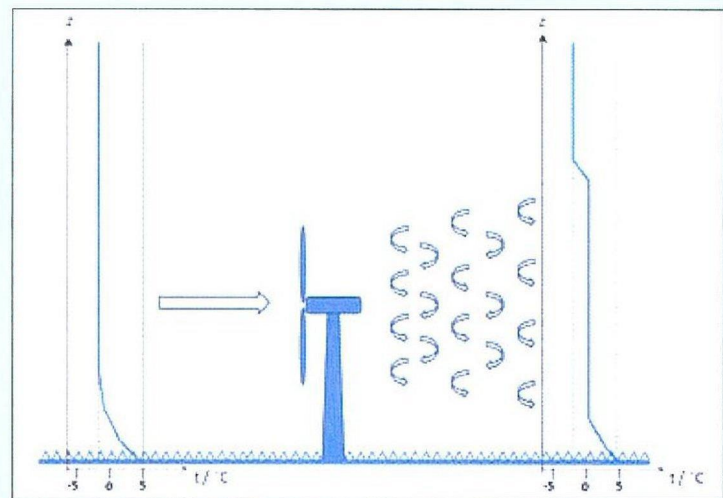
12, 12 UTC at Emden, Germany, at the North Sea coast gave a temperature of -1.5°C and a relative humidity of 99 % 28 m above ground. The ascent at Schleswig at the Baltic Sea coast indicated the presence of a completely saturated air mass up to a height of nearly 600 m above ground on 00 UTC of February 12. The ascent at Ekofisk on 12 UTC of that day gave fully saturated air of 4 °C and southerly flow of 8.5 m/s at 29 m above the sea level. Radiosonde data have been obtained from www.weather.uwyo.edu/upperair/sounding.html. The satellite image for this day showed a large extended fog patch over Denmark, Northern Germany and the eastern part of the North Sea which fitted well to the high relative humidity measured on that day.

The sea surface temperature near Horns Rev was around +5°C in the week ending on February 12, 2008 (data from the German Federal Office on Maritime Travel and Hydrography (BSH) www.bsh.de/de/Meeresdaten/Beobachtungen/ Meeresoberflaechentemperatur/). This meant that foggy, nearly saturated cold air with a temperature slightly below freezing point was advected that morning from the Danish and German coast to the about 6 degrees warmer North Sea.

Explanation of the Formation of the Wake Clouds

The advection of this colder air over the warmer sea surface leads to the formation of a shallow layer with sea smoke. This sea smoke is visible all over in Fig. 1 upstream of the wind farm and even between the banners of wake clouds. The left-hand temperature profile in Fig. 5 gives an explanation of this phenomenon. If we assume that nearly saturated air (99 % relative humidity) of -1°C flows over a likewise moist layer directly over the water surface with +5°C and 99 % humidity, then due to buoyancy forces a shallow mixed layer forms within which the temperature decreases with height from 5°C at the sea surface to -1°C in the air above (indicated by the vertical dashed lines in Fig. 5). Within the temperature range between 0°C and 4°C (see Fig. 3 and the vertical grey bars in Fig. 5) the formation of mixing fog or sea smoke can be expected. Comparing blade length and hub height of the turbines visible in Fig. 1, this sea smoke layer is only five to ten metres deep.

Using Magnus' formula given in Section 2 above, it can be calculated that perfect mixing of equal amounts of air with 99 % relative humidity having -1°C (water vapour pressure e = 5.616 hPa) and +5°C (e = 8.664 hPa) leads to a mixed air mass with +2°C and a water vapour pressure of e = (5.616+8.664)/2 = 7.140 hPa). The saturation water vapour pressure E at 2°C from Magnus' formula is only 7.065 hPa (see dashed line in Fig. 3). Therefore the mixed air is over-saturated with 101.1 %.

The situation in Fig. 1 changes dramatically, when the air passes the first row of turbines. A possible temperature profile in the wake region is given by the right-hand temperature profile in Fig. 5. The turbulence produced by the turning turbines leads to a nearly perfect vertical mixing of the air within the wake. When the lower edge of the wake spreads into the warmer air layer below, air from this layer is included into the mixing process and the temperature in the wake starts to rise. When it rises more than about one degree, then the temperature in the wake enters the range marked by the grey bar in Fig. 5 and condensation starts and the wakes become visible. With the spreading of the wakes further away from the turbines the wake clouds become wider. The overall unstable temperature stratification of the air (warmer air underneath colder air) leads to the slightly bumpy nature of the wake clouds. They look like small cumulus clouds.

Conclusions

The analysis above has proven that the weather conditions on February 12, 2008 were sufficient for the formation of mixing fog in the wakes of the turbines of Horns Rev wind farm. This phenomenon requires the existence of two layers of air with two different temperatures and both with very high relative humidity very close to saturation. The separating line between these two layers must be close to the hub height. Then, the mixing of these two layers will lead to the formation of mixing fog. Such a situation is most likely to form during advection of air from land to sea or vice versa. A comparable mixing-fog phenomenon is the formation of cloud banners behind mountain crests shortly after rain events when cold and very humid air aloft mixes with warmer and likewise very humid air which is vented upwards in a lee vortex on the downstream side of the crests.

Due to the necessary requirements for formation (existence of two layers with considerably different temperature with the separation line between the two layers close to the hub height of the turbines and very high relative humidity in both layers), it can be assumed that the formation of such wake clouds is a rather rare event. The most likely area for such phenomena is a stripe on both sides of a coast line with the sea and land having considerably different surface temperatures and winds crossing the coastline.

References

Emeis, S., 2000: Meteorologie in Stichworten. Hirt's Stichwortbücher, Gebrüder Borntraeger Stuttgart. XIV+199 S. ISBN 3-443-03108-0.

Wake effects at Horns Rev and their influence on energy production

Martin Méchali[1][*], Rebecca Barthelmie[2], Sten Frandsen[2], Leo Jensen[1], Pierre-Elouan Réthoré[2]

[1]Elsam Engineering (EE)	[2]Risø National Laboratory (Risø)
Kraftværksvej 53	Frederiksborgvej 399
DK-7000 Fredericia	DK-4000 Roskilde
Ph.: +45 79 23 31 66	Ph.: + 45 46 77 50 20
mame@elsam-eng.com	r.barthelmie@risoe.dk

[*]Corresponding author

1.   Abstract

In recent years a number of programs have been carried out with the purpose of investigating wake effects at Horns Rev offshore wind farm. The latest Danish project "Large wind farms shadow: measurements and data analyses" aims to map the downstream effect of large wind farms, and includes monitoring the in-park wake effects. The wind farm considered, Horns Rev, has an installed capacity of 160 MW. Approximately one years data are available after the final completion of the Horns Rev turbines, this paper presents the first analysis based on a large amount of data from the Horns Rev wind farm in operation.

The data for the current paper are acquired partly from the meteorological masts positioned north west and east of Horns Rev and from the SCADA database, which contains all observed data from the turbines at both wind farms.

This paper presents analysis of the power output in a row of operating turbines and the dependency on wind direction relative to the row direction. The aim is to describe the magnitude of the wake effects and give an indication of the importance of wind direction. For the majority of the selected cases the turbines were operating at wind speeds with high rotor thrust. Comparison of the results for different spacing at Horns Rev (along rows and columns and for diagonal spacing) will provide insight to the mechanism of wake development and expansion.

Part of the project involves development of a model based on the analytical solutions of wake development described by Frandsen et al. (2004). This model is currently being operationalised Horns Rev and results from the modelling will be compared with the data analysis. The objective is to illustrate whether the merging of wakes within large wind farms can be described by simple linear models or whether the inclusion of the two-way interaction between the wind turbines and the boundary-layer is a necessary prerequisite for accurate models of wakes to be used in future wind farm design.

2.   Introduction

To increase the understanding of the wake effects from large wind farms a number of projects are currently being carried out with the purpose of describing and quantifying wakes. Especially the economical aspect has been an important driver in this project, since an improved ability to predict wake losses may improve the feasibility of large wind farms significantly.

Horns Rev wind farm is particularly interesting for future offshore projects since it is to some degree similar to a number of proposed wind farms: It is a large matrix spaced with 7 rotor diameters and it has a long land fetch of approximately 14km.

The wind farm consists of 80 Vestas V80 turbines with 2MW generator and 70m hub height. It is laid out in a matrix with 8 rows (east-west) and 10 columns (north-south).

Since the wake effect modelling is still in its early stages the current project is limited to focus on wakes in situations where the wind is aligned with the rows of the wind farm as shown in figure 2.1.
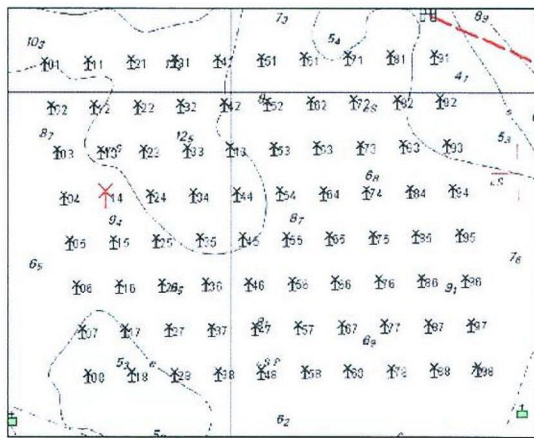
Figure 2.1 Wind farm layout

Although other papers (for example Jensen, Leo et al. [1]) have presented similar analyses of the Horns Rev data the present work is the first covering a large amount of valid data, which allows a higher degree of statistical independency.

The available data tends to decrease significantly as the necessary criteria are applied. An example of such criteria may be: narrow wind speed and wind direction intervals and all turbines in a row are in operation. It is obvious that very specific analyses require a very large set of data to provide reasonable results.

3. Data

The data is taken partly from the SCADA database, which is continuously updated with turbine performance parameters and partly from the met. masts close to the wind farm. The met. masts are positioned as shown in figure 3.1 with M2 northwest of the wind farm and M6 and M7 east of the wind farm. M6 and M7 were initially erected to facilitate measurements of the wake effects behind the wind farm (in the predominant western wind direction), whereas M2 should be in free stream at nearly all times.

Due to downtime of the measuring system at M2 it has been necessary to use a large amount of data from the M6 mast although it is often in wake from the wind farm. However, since it concerns mainly the wind vane it is assumed that the error committed is acceptable, as the wind farm is not expected to impose a general change of wind direction downstream.
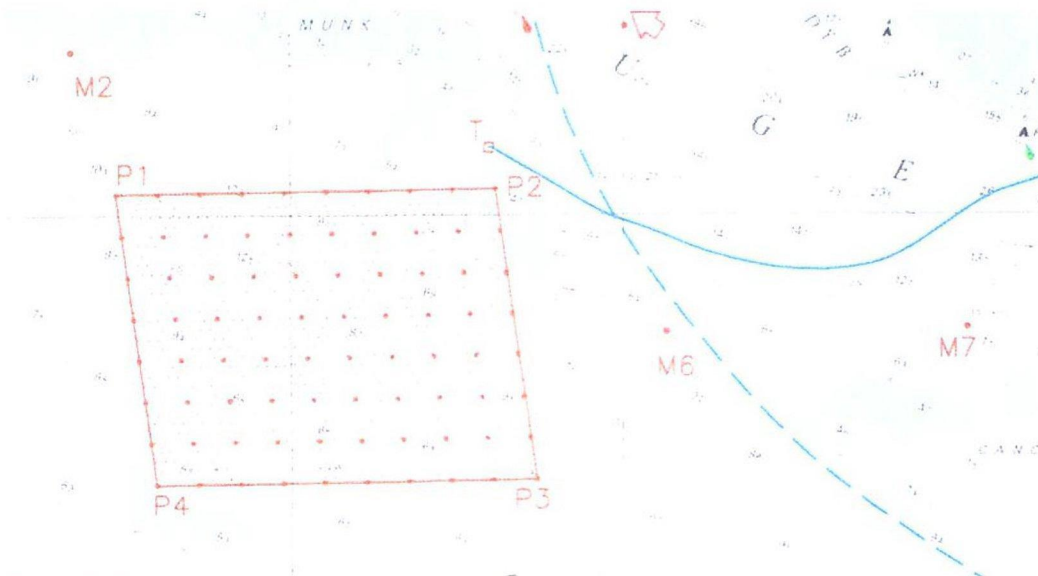
Figure 3.1 Wind farm and met. mast positions

All data are acquired as 10-min means and information from the mast and the SCADA system is combined in one file containing all data for the analyses. The period with valid data ranges from 1-1-2005 to 31-12-2005 and has a recovery rate of approximately100%.

To ensure that a large amount of data is available for the analyses only the border rows and columns are excluded i.e. for west wind situations the first and eighth rows are left out.

4. Wake modelling

The analytical model derived by Frandsen et al. (2006) [3] links the small scale and large scale features of the flow in wind farms. The model currently handles regular array-geometry with straight rows of wind turbines and equidistant spacing between units in each row and equidistant spacing between rows. Firstly, the case with the flow direction being parallel to rows in a rectangular geometry is considered by defining three flow regimes. From the upwind end of the wind farm, the model encompasses three regimes as illustrated in Figure 4.1: In the first regime, the wind turbines are exposed to multiple-wake flow and an analytical link between the expansion of the multiple-wake and the asymptotic flow speed deficit are derived. The second regime materializes when the (multiple) wakes from neighbouring rows merge and the wakes can only expand vertically upward. This regime corresponds (but is not identical) to the flow after a simple roughness change of terrain. The third regime is when the wind farm is "infinitely" large and flow is in balance with the boundary layer.
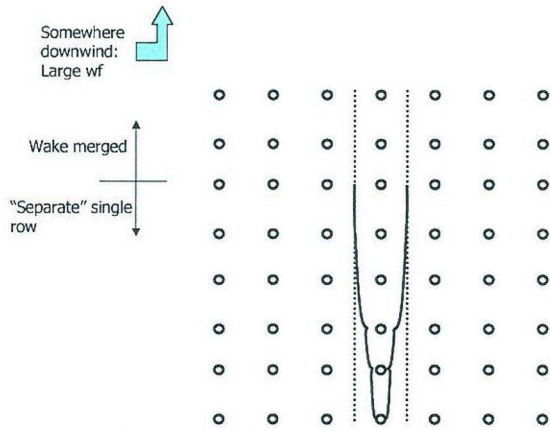
Figure 4.1. Illustration of the regimes of the analytical model. The flow is parallel to the rows of wind turbines.

In brief the expansion of the wake behind a wind turbine is given by the general solution:

$$D_x = \left(\beta^{n/2} + \alpha \cdot s\right)^{1/n} D_0, \qquad s = x / D_0,$$

where the solution for n has been suggested as 3 by e.g. Schlichting (1968).

α is the decay constant which is related to the thrust coefficient C_T and β is the initial wake expansion, also being calculated from the thrust coefficient:

$$\beta = \frac{0.5 \cdot (1 + \sqrt{1 - CT})}{\sqrt{1 - CT)}}$$

Figure 4.2 shows results for the single/multiple wake model which does not account for turbine wake interactions with the ground. By adjusting parameters in the model it is possible to get a good fit to the observed data. Notably, the exponent parameter was chosen as $n=1$, which choice provides the excellent fit for the first few units. At the end of the row, the model recovers too well, which is expected: with the chosen way of modelling the asymptotic value of n for increasing wind turbine number must be ½ to ensure a non-vanishing wind speed deficit.
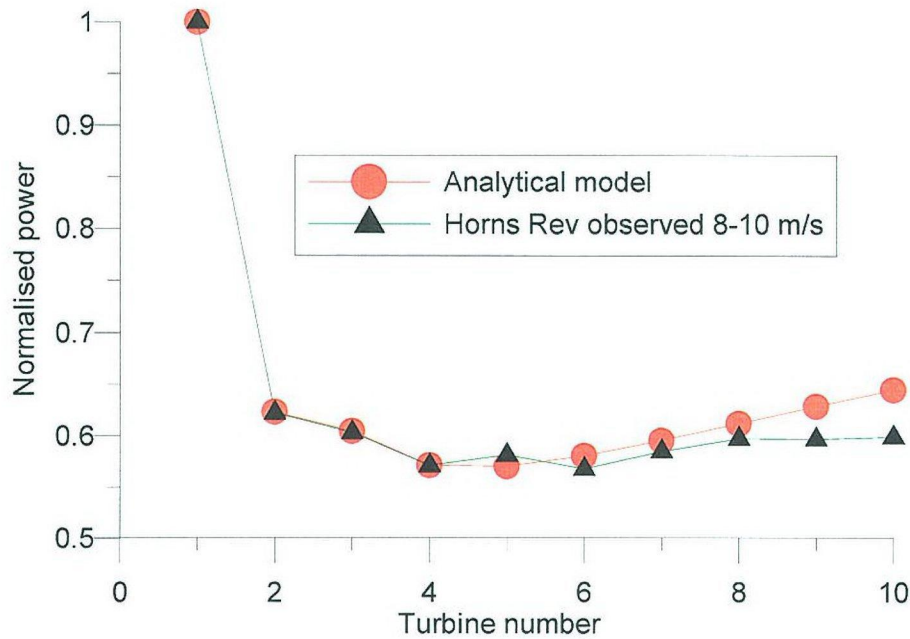
Figure 4.2 . Comparison of single wake model with observations for Horns Rev.

5. Results

Seeking applicable data in a data set like the current one faces a dilemma: use a large amount of information to allow statistical independency by having wide wind direction sectors for each case or narrow down the sectors to see the exact wake effects for each direction.

In the section below the difference between these approaches and their results are shown.

5.1 Wind along the row with wide direction sector

The rows 2 through 7 are analysed using a 30 degree wide sector ranging from 255° to 285°. The wind speed interval is chosen to be between 7 and 10m/s as this is where the power is relatively high (although not full load) and the thrust coefficient has not dropped significantly as at high wind speeds.

There are several ways to define the wind speed: Either using the wind speed from one of the masts or calculating the wind speed from the power of one of the front line turbines. Basically one should expect that the most reliable solution would be to calculate wind speed from the output power as this would reflect the wind speed in the wind farm rather than some kilometres away. However, results show that the standard deviation of the results becomes much larger using this approach rather than taking the wind speed from the M2 mast. Therefore in the following the wind speed is taken from M2 and wind direction from M6 (due to the already mentioned downtime of the measuring system).

The observed wake effect is plotted for this situation represented by the relative power drop of each turbine in the row. It is obvious that the largest relative power drop is observed from turbine 1 to turbine 2, whereas the power drop from turbine 2 to turbine 10 is smaller than between the first 2 turbines. The plots are separated in 1m/s intervals.
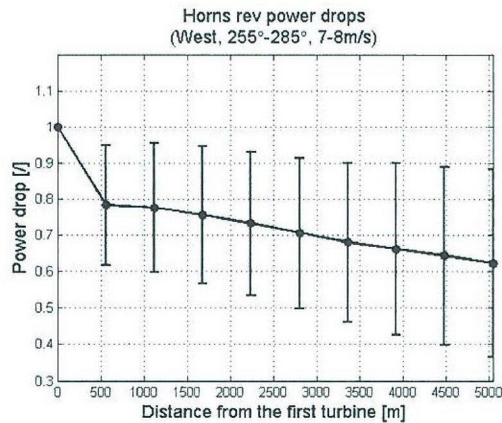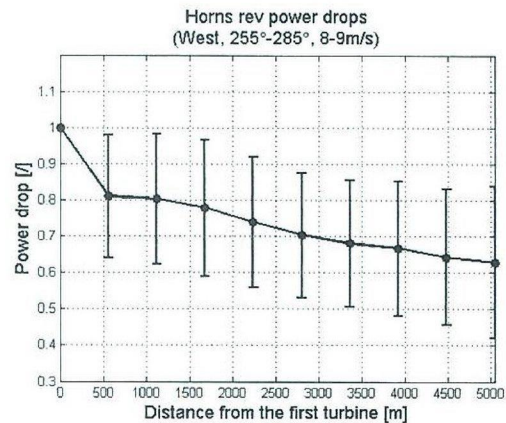
Figure 5.1 Relative power drop 7-8m/s

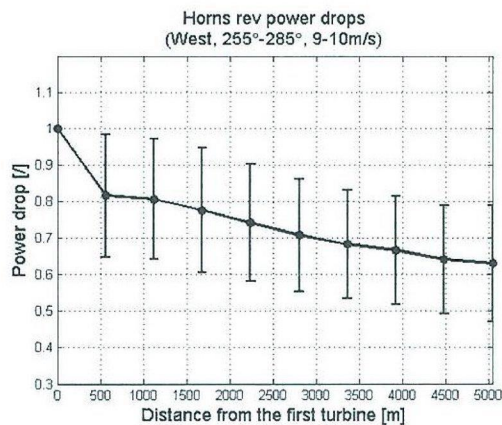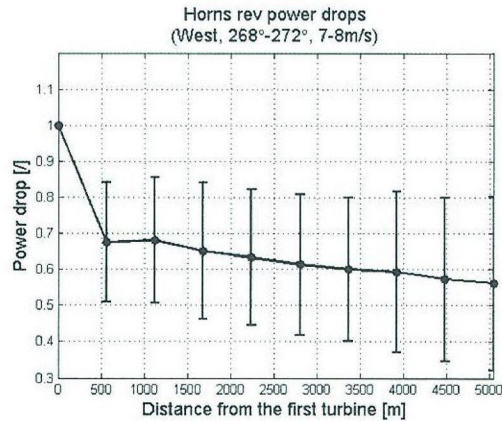Figure 5.2 Relative power drop 8-9m/s

Figure 5.3 Relative power drop 9-10m/s

Besides observing the mean value down the line of turbines it is quite interesting that the standard deviation of the results (represented as a vertical line at each mean value point) is very large for all cases. This indicates that the results cover very different situations.

There are several possible reasons for the large deviations and these should be checked individually (turbulence, wind shear and wind direction dependency). One of the more likely reasons is that the results cover more than one phenomenon or physical condition of the wake; therefore this is looked more into in the following section.

5.2   Wind along the row with narrow direction sector

To try and separate the different situations the wind direction sector is narrowed down to +/- 2°. The remaining conditions are similar to the ones in section 5.1. This means that the data extracted for this analysis are included in the former investigation.

The plots are shown below:

Figure 5.4 Relative power drop 7-8m/s
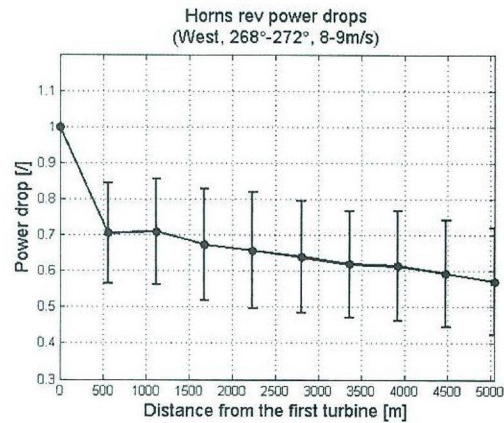
Figure 5.5 Relative power drop 8-9m/s
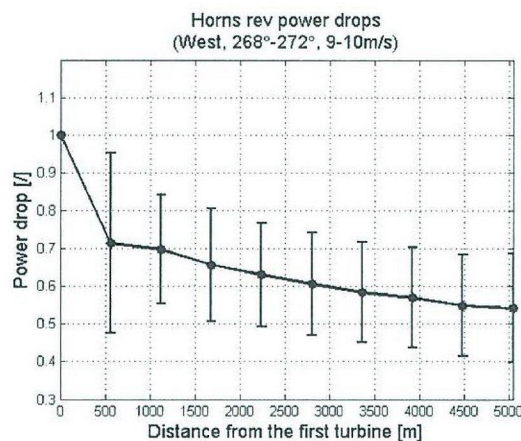
Figure 5.6 Relative power drop 9-10m/s

The results show that there is a significant change in the wake effect when the wind is limited to being parallel to the row direction (or very close to it). The power drop from turbine 1 to turbine 2 has increased from an average value of approximately 0.2 to about 0.3. This indicates that the very large power drops between the first two turbines described in earlier papers (for example Jensen, Leo et al.) only occurs in a very narrow sector around the row direction. At other wind directions the power drop is significantly smaller from turbine 1 to turbine 2.

For the remaining turbines the pattern is almost the same for the two analyses: the power drop from turbine 2 to turbine 10 is between 0.15 and 0.2, which occurs in an almost straight line.

The natural conclusion to this difference between wake effects for flow parallel to the row and wind direction being slightly off the row direction is that a wake model must be able to give significantly different results for even small changes in wind direction.

Unfortunately the standard deviations of the results are still very large and they have not decreased by narrowing the wind direction sector, so it is possible that another factor is causing the different situations and that sorting the data according to this factor might give lower deviations.

In earlier work, situations have been shown where the power output from the turbines increases down the line (for the last 4-5 turbines). Of course these situations are still present, however the mean results show that the general tendency is a large power drop from turbine 1 to turbine 2 and a steadily decreasing power output along the line of turbines. When creating a new wake model it has to be decided whether it should be able to predict all situations or simply have the ability to present the mean results correctly. This of course is question of the purpose of the model – does it aim at scientific or industrial use?

5.3   Wind along a diagonal

The diagonal in the wind farm allows an investigation of wake effects at a larger distance between the turbines. For Horns Rev the distance between turbines in the south-west to north-east diagonal is 9.3D (740m). To compare results with the data in the section 5.2 the must be a maximum number of turbines in the diagonals. Given the layout it is

possible to find 3 lines with 8 turbines. Compared to the former section the present has less data since only 3 lines can be assessed (for western wind direction 6 lines are available).

The analysis has been performed with similar input data as in section 5.2 i.e. the wind direction interval is +/- 2° and mean wind direction is 222°.

The plots are shown below:

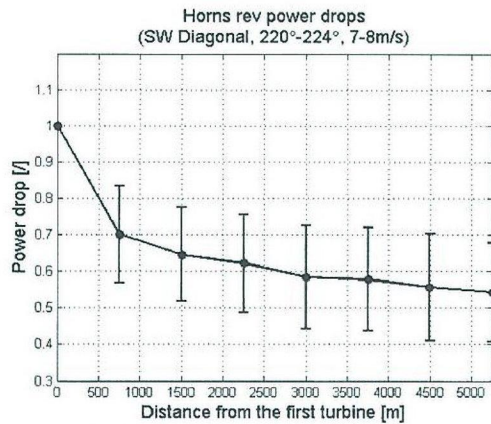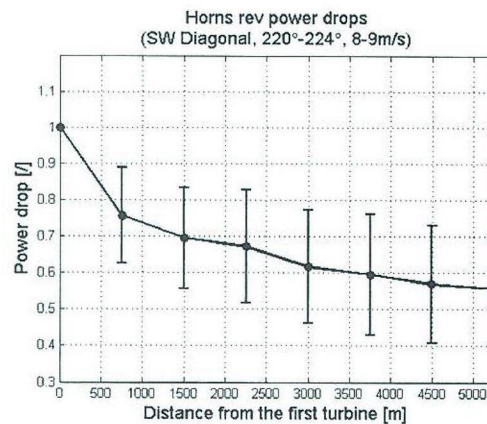*Figure 5.7 Relative power drop 7-8m/s*
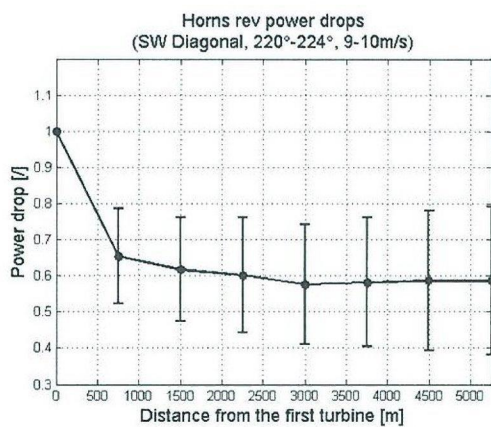

Figure 5.8 Relative power drop 8-9m/s

Figure 5.9 Relative power drop 9-10m/s

It is quite obvious that the data basis is smaller for this analyses compared to the former. Especially for the 8-9m/s case there are very few data resulting in a large standard deviation.

Despite the inaccuracies in data mean values it is assumed that the data set may be used for investigating general tendencies.

To compare the results data is plotted for each of the analysed wind speed intervals.
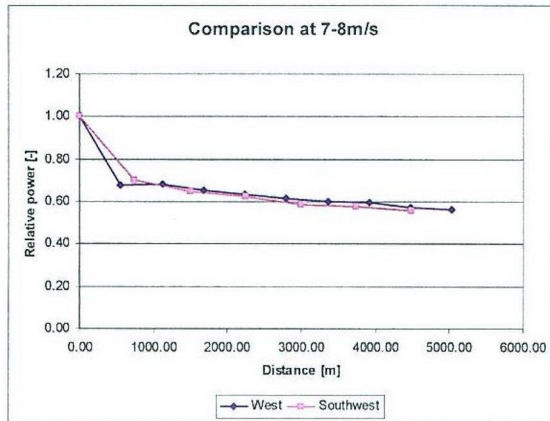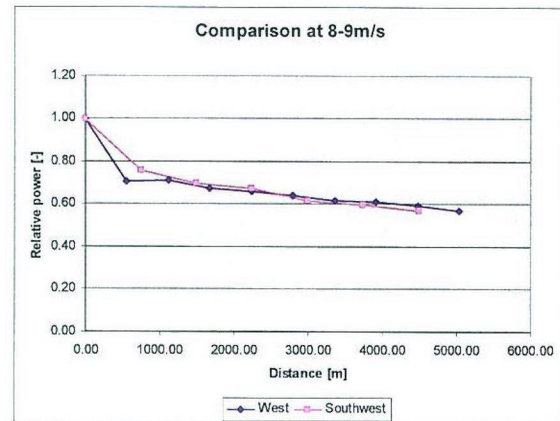
Figure 5.10 Power drop comparison 7-8m/s

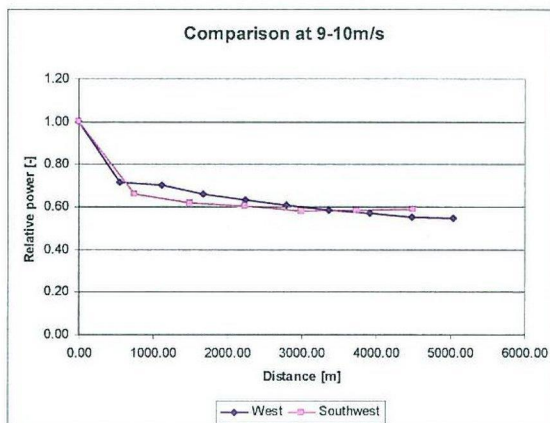*Figure 5.11 Power drop comparison 8-9m/s*

Figure 5.12 Power drop comparison 9-10m/s

The initial conclusion here is that the differences are relatively low and the power drop from turbine 1 to turbine 2 is very significant for both cases. Generally the power drop between the first two turbines is largest at 7D spacing (for the lower wind cases), and for the next 3 turbines the power drops of almost equally. After this there seems to be an obvious difference between the 7D and the 9.3D case at 9-10 m/s: For the 9.3D case the power output levels out from turbine 5 and is almost constant for the remaining turbines in the row. This indicates that the size of the "infinitely" large park depends on the distance between turbines in the wind farm. It also shows that the infinitely large wind farm is achieved at a fairly limited number of rows in the wind farm.

5.4   Directional dependency

If differences are experienced in the data for shifting wind directions it must be analysed what causes this effect. For example a short land fetch may cause changes to wind shear and turbulence compared to when the land fetch is practically infinite. In this section the results of section 5.2 are compared with similar results with wind from coming from east.
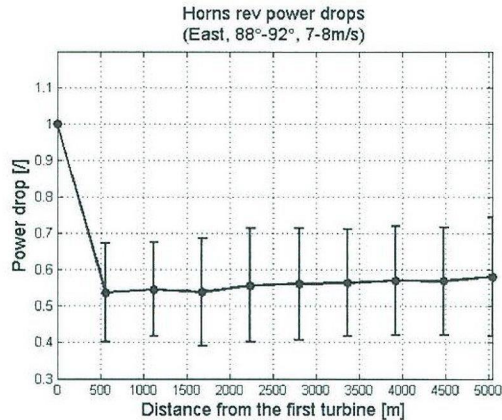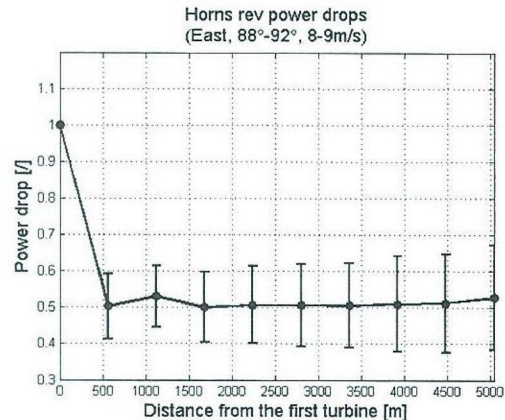
Figure 5.13 Relative power drop 7-8m/s
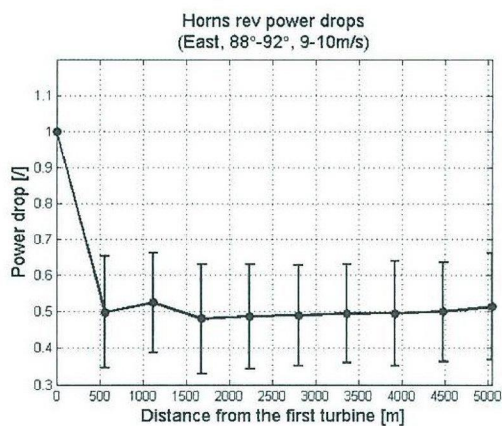

Figure 5.14 Relative power drop 8-9m/s

Figure 5.15 Relative power drop 9-10m/s

The most obvious differences between these results and the ones in section 5.2 are the very large power drop from turbine to turbine 2 and the slightly increasing power towards the end of the line. There are several possible explanations to this and the most probable ones are described below:

The land fetch of 15km to the east may cause different wind conditions such as wind shear and turbulence, which has a different effect on the power output.

Another very possible explanation is that the difference is caused by the difficulty of describing the wind direction for the entire wind farm by one single measurement, which is positioned very far from the western turbines. It has already been established that the power drop is not as significant for wind directions slightly off the line direction as it is when the wind is straight down the line. When using a wind direction measurement far from the first lines of turbines it is quite possible that the wind direction at the turbines is not always straight down the line as predicted by the wind vane at the met mast 5km away. This would give some cases with lower power drop between turbines 1 and 2 and eventually cause a larger mean value of the mentioned power drop. This case with first rows of turbines being far from the met mast occurs when wind is coming from the west (see section 5.2).

When wind is coming from the east the first rows of turbines are relatively close to the met mast and the chance that they experience the same wind direction as the mast is quite large. This means that the power drop from turbine 1 to turbine 2 will be occurring when wind is coming straight down the line for the majority of the cases. The result is that the power drop for this direction is likely to be larger (on average) than what was found for the west wind case. In figures 5.13 through 5.15 this is exactly what is found compared to the figures of section 5.2.

Another indication that this explanation is plausible is that the average power seems to be increasing towards the end of the line. If the turbines furthest away from the met mast are sometimes experiencing another wind direction they will not be in direct wake and therefore the power output from these turbines will be larger than the ones upwind. The effect is the exact same as seen in west winds.

Alternatively there might be horizontal gradients in the wind speed increasing as flow moves offshore (i.e. from east), which are slightly counteracting wake losses.

One last factor that seems to have an effect on the wake loss is the atmospheric stability. Recently an investigation of the wake loss pattern has been compared to the simultaneous temperature difference between air at 62m and water at

sea level. As this difference is assumed to give a good indication of the stability the analyses concludes that this factor does influence the wake effects. Furthermore the mean stability varies from one wind direction to another, which means that different directions will have different wake conditions and thereby the same results cannot be expected for the eastern and western winds.

6. Conclusion

The conclusions to the work done for this paper relate to the results and to the proposed model for wake calculations. As in earlier work large power drops were experienced for wind directions where wind is parallel to the wind turbine rows, however compared to the governing conviction a power drop from 100% to 50% between the first two turbines must be considered extremely large.

The analyses also showed that the direction and where it is measured is very important for the results. It is difficult to use one wind direction for the entire wind farm especially for the turbines far from the mast. This implies that there is no such thing as steady state for a physical system of this size and it must be expected that the wind will always vary from one point in the wind farm to another causing the data points to be scattered. One has to accept that working with wind farm data is a statistical process that implies a significant spread in the data basis.

It is shown that the very significant power drop occurs in a very narrow sector around the line direction and once wind is not straight down the line the power drop decreases fast with direction.

A good agreement was found between data from the east-west rows (in west wind) and the southwest diagonal (in south-west wind) although it seems there is a tendency for the power drop to become almost constant towards the end of the wind farm for the diagonal case. This implies a balance between the wind farm and the boundary layer above it.

There are strong indications that atmospheric stability has an influence on the wake phenomena and that the stability is strongly dependant on the wind direction, although the wind farm is placed far offshore.

Generally the model is able to predict the mean power drop from turbine 1 to turbine 2 in the row (when wind is parallel to the wind turbine row) after finding suitable model parameters. Towards the end of the wind farm the model is slightly over predicting production, as the energy recovery seems to be too large.

7. Acknowledgement

8. References

[1] Jensen, L., Mørch, C., Sørensen, P., Svendsen, K. H.: "Wake measurements from the Horns Rev wind farm". EWEC 2004, 22-25 November 2004, London, United Kingdom.

[2] Barthelmie, R., Frandsen, S., Jensen, L., Mechali, M., Perstrup, C.: "Verification of an efficiency model for very large wind turbine clusters". Copenhagen Offshore Wind Conference 2005. 26-28 October 2005, Copenhagen, Denmark.

[3] Frandsen, S., Barthelmie, R.J., Pryor, S.C., Rathmann, O., Larsen, S.E., Højstrup, J., Thøgersen, M.: "Analytical modelling of wind speed deficit in large offshore wind farms". Wind Energy, Published Online: 11 January 2006 (in press).

Wake measurements from the Horns Rev wind farm

Leo E. Jensen, Elsam Engineering A/S
Kraftvaerksvej 53, 7000 Fredericia
Phone: +45 7923 3161, fax: +45 7556 4477
Email: leje@elsam.com

Christian Mørch, Elsam Engineering A/S
Email: chrm@elsam.com

Paul B. Sørensen, Elsam Engineering A/S
Email: pbs@elsam.com

Karl Henrik Svendsen, Vestas Wind Systems A/S
Email: khs@vestas.dk

Summary

Horns Rev is a large offshore wind farm exposed to low turbulence flow. It has a layout and a location which makes it excellent for general studies of wake effects. Three met masts are installed around the wind farm area to study the recovery of the wake flow behind the wind farm and support the development of new scientific and engineering models for calculation of external wake effects from large offshore wind farms.

All wind farm operation data is stored by a SCADA system. The SCADA system collects data from more than 200 sensors every 10 minutes. This data is used for the analysis of internal wake effects.

Wind speed and turbulence has been analysed for three lines of turbines - two aligned and one diagonal line of turbines. The analysis shows that there is a large reduction in wind speed from the first turbine to the second in a row, but that the wind speed does not change much from the second to the tenth row.

The wind data from the wake masts show that there is still a clear influence of the wind farm 6 km downstream on both mean wind speed and turbulence. The wake masts also indicate that the boundary layer has still not stabilized at pure offshore conditions even though the fetch is more than 15 km.

**Key words: offshore, wind farm, turbulence, wake**

This is a paper on wake measurements from the Horns Rev wind farm. We are of the impression that a presentation of these measurements is of great interest to the scientific community.

From a scientific point of view, the Horns Rev wind farm is very interesting for the following reasons:

- It is an offshore wind farm being exposed to low turbulence flow that has an absolute minimum disturbance from the underlying surface
- It has a very regular shape and layout that is perfectly suited for general studies
- It is fairly large, enabling studies of large wind farm objects
- It will be exposed to wind from all possible wind directions

The wind farm

The wind farm layout is a 10 times 8 matrix forming a slightly oblique rectangle. The distance between the turbines is 560 meters in both directions, corresponding to 7 rotor diameters.
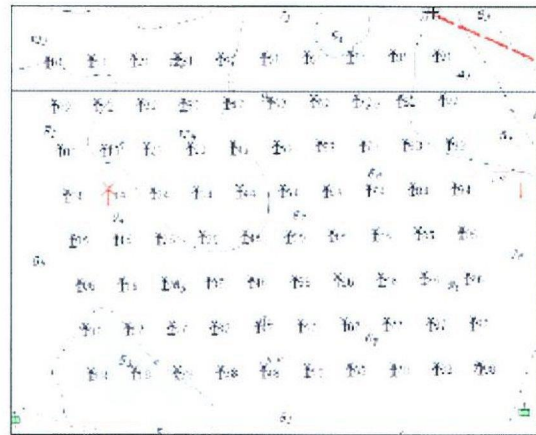

The turbines are numbered so that the westernmost column is numbered from 01 to 08 with 01 being the turbine in the northwest corner, and the easternmost column being numbered 91 through 98. This may lead to the wrongful assumption that there are actually 98 turbines, but as several numbers are unused, the number of turbines is still only 80.
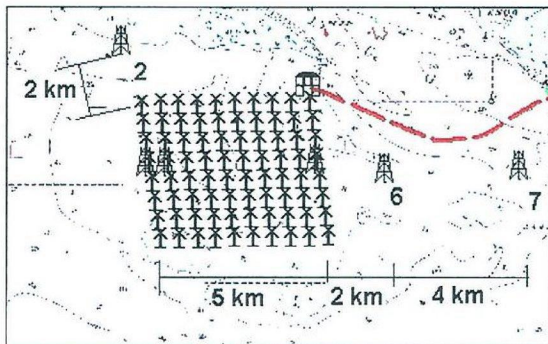
Referring to UTM zone ED32, the co-ordinates of the corner turbines in the rhombus are:

01: 423974, 6151447	91: 429014, 6151447
08: 424386, 6147543	98: 429431, 6147543

The wind farm is located in the North Sea, approximately 30 km west of Esbjerg. The distance to the nearest point on shore (Blåvands Huk) is approximately 13 km.
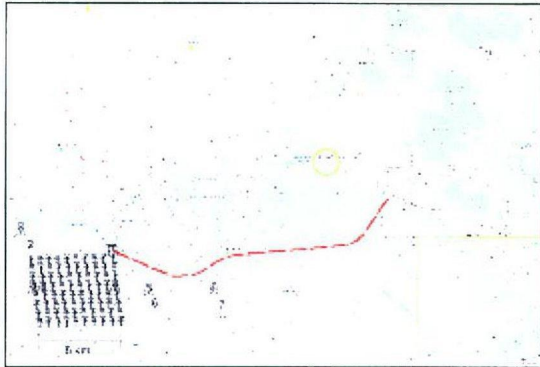
Around the wind farm three met masts are installed.

The oldest mast is called M2. This mast was installed before construction of the wind farm and is the one that was used to determine the wind resource at the site. Several other papers have described and analysed measurements from that mast.

In the summer of 2003 two more masts (called M6 and M7) were installed. The purpose of these masts is to study the recovery of the wake flow behind the wind farm for westerly winds, and support the development of new scientific and engineering models for calculation of external wake effects from large offshore wind farms.

Referring to UTM zone ED32, the co-ordinates of the three masts are:

Mast	X co-ordinate	Y co-ordinate
M2	423412	6153342
M6	431253	6149502
M7	435253	6149502

Plotting of these co-ordinates will show that M2 is located 2 km north-northwest of the northwest corner turbine (01). M6 and M7 are located 2 and 6 km east of the wind farm respectively on a line that passes right through the middle of the fourth and fifth row.

The wind turbines
The wind turbines are all of the Vestas V80 type shown in the picture below. Please do not pay too much attention to the fact that the turbines are not operating and do not agree on the wind direction. This picture was taken just after the construction, and at that time the turbines were not allowed to go into normal operation yet.

The dimensions of the turbines are shown in the sketch below.
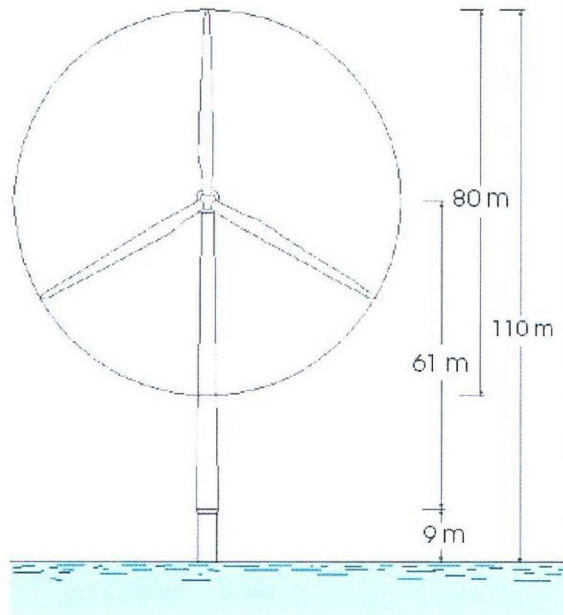
For the wake measurement, the most interesting turbine data are the diameter, the hub height and the thrust coefficient. When using the Vestas V80 turbine in wake modelling tools, the values for power and thrust coefficient listed below can be applied.

Wind speed	Electric Power (kW)	Thrust coefficient
4	66.6	0.818
5	154	0.806
6	282	0.804
7	460	0.805
8	696	0.806
9	996	0.807
10	1341	0.793
11	1661	0.739
12	1866	0.709
13	1958	0.409
14	1988	0.314
15	1997	0.249
16	1999	0.202
17	2000	0.167
18	2000	0.14
19	2000	0.119
20	2000	0.102
21	2000	0.088
22	2000	0.077
23	2000	0.067
24	2000	0.06
25	2000	0.053

As the Vestas V80 turbine is a pitch-variable speed machine, running constant tip-speed ratio at low to medium wind speeds, the thrust coefficient is fairly constant. This is very convenient for the scientific work as e.g. relative wind speed deficits can be expected to be fairly constant for a large wind speed range.

Please note that the power and thrust coefficient curves are specific to the turbines delivered for the Horns Rev wind farm and may not apply to V80 turbines delivered for other projects.

The wind farm main controller
A feature, which is not so convenient for the scientific work, is the wind farm main controller.

This is a new feature installed on the Horns Rev wind farm that enables the operator to control the power output of the wind farm. Of course the operator cannot extract more power from the wind farm than what is present in the wind but the power output can be reduced periodically if so desired. The strength of this feature is the speed of change in power output. The Horns Rev offshore wind farm can produce gradient measured in MW per second, where traditional power stations measure in MW per minute.
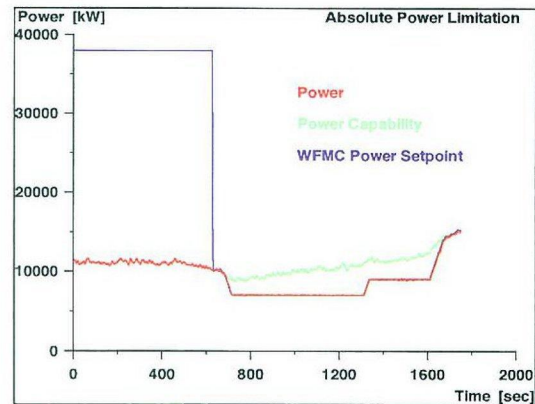
For the purpose of scientific work on wake effect, however, this is a major disturbance of the otherwise nice and flat thrust coefficient curve. Operating the main controller will make it practically unpredictable, and the data from those periods will have to be sorted out.

Internal wake effects observed
All data about the wind farm operation is collected and stored by a Surveillance, Control and Data Acquisition system (SCADA). It operates on an ethernet connection between the wind farm and a database server in Esbjerg.

On this server values from more than 200 different sensors are stored every 10 minutes. This adds up to a large amount of data. The database has at least 300 Gb disk space and is continuously expanded.

These data are used for the analysis of internal wake effects.

In the analysis of both internal and external wake effects, however, the availability of the wind farm is

just as important as it is for the economy of the installation. As the availability at Horns Rev - due to transformer and generator problems - has not yet reached the required level, this has been an issue given special attention in the data presented here as well. Some types of analysis, such as the array efficiency of the entire wind farm simply does not make sense at the present stage, since too little data is available with all turbines in operation at the same time. But other interesting phenomena can still be observed.

The types of analysis selected for this paper are:

- Analysis of shelter in individual rows
- Analysis of spread of wake effects
- Analysis of local speed up

Even with the transformer and generator problems it is still possible to get a good idea of the reduction of wind speed along a single line of turbines. Four different lines have been selected for analysis.
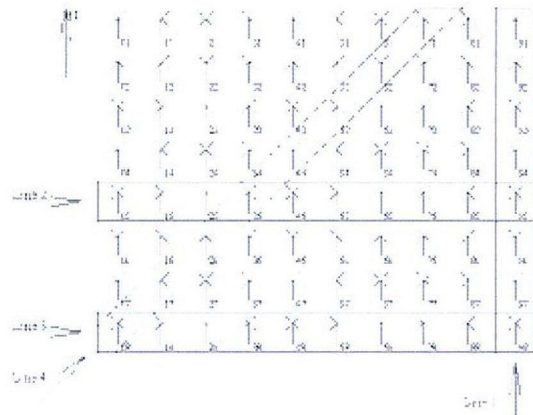
Line 1 is a line on the eastern boundary of the wind farm.

Line 2 is an east-west going line approximately in the middle of the wind farm.

Line 3 is a line on the southern boundary of the wind farm

Line 4 is a diagonal line from the southwest towards the northeast. This line differs from the three others in the distance between the turbines being larger, and the perpendicular distance to neighbouring turbines being smaller.

The wind directions used for the analysis have been taken from the recordings at M2 (northwest of the wind farm). This tends to produce slightly unstable results for line 1, which is probably partly due to the distance and partly due to disturbances in the general flow from the wind farm. Therefore results from line 1 are not shown here.

The wind directions to be used for the individual lines are shown in the table below. The small deviation

from pure west is due to the fact that the turbine rows are aligned with the UTM co-ordinate system, which at that location has a deviation from true north of 1 degree.

Line	Direction
Line 1	172.0
Line 2	269.0
Line 3	269.0
Line 4	220.4

Line 2
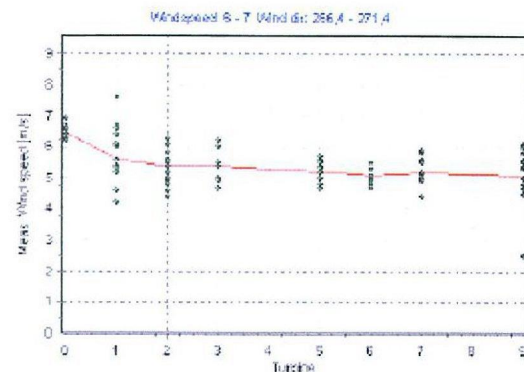
The data presented in the above plot is wind speed measured on the nacelle anemometers. These anemometers are calibrated to account for the disturbance by the nacelle and rotor, and comparisons with the individual power curves indicate that they are fairly accurate.

The graph is for wind speeds between 6 and 7 m/s on the westernmost turbine, and shows the reduction in a very narrow wind direction sector. As the graph shows, the general tendency is a large reduction from the first to the second turbine, but it also shows that the sheltering effect further downstream seems to stabilize at a constant level.

The largest scatter is seen on the second turbine (1), where a single observation indicates that situations with speed-up in the second row of turbine can be found in special conditions.

The fact that there are no dots for turbines 4 and 8 indicate that no information was available in the SCADA database. During that period this normally means that the turbine has no power due to a faulty transformer, but it could also just be a communication failure between the turbine and the SCADA system.

Line 3
The next plot shows the same situation on line 3. It shows very much the tendency with regard to the average wind speed reduction being large at the second and fairly constant for the rest of the row. The scatter, however, is significantly larger.

Windspeed 6 - 7 Wind dir 268,4 - 271,4
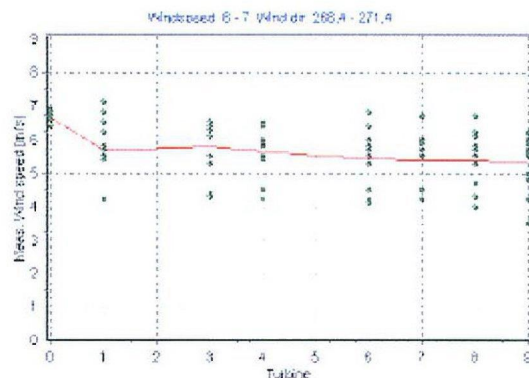
The larger scatter is probably caused by the fact that the turbines are more exposed to free inflow during the turbulent variations of the wind directions.

Line 4

Windspeed 10 - 11 Wind dir: 217,89 - 222,89
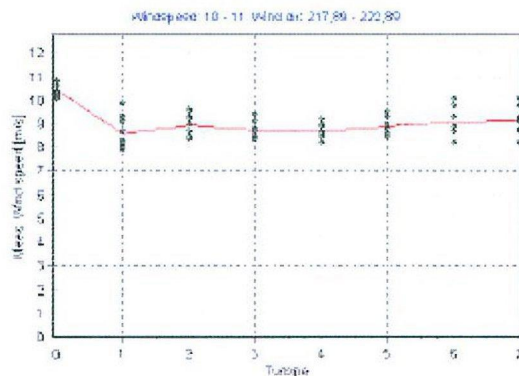
Also in line 4 (the diagonal line) the tendency is the same. The most significant difference here is that the spread of the observations is significantly smaller than in both line 2 and 3. This indicates that from this wind direction the wakes actually merge with wakes from the neighbouring rows, forming a more uniform flow for the turbines.

If we compare the wind speed reduction in line 2 (which is aligned) and line 4 (the diagonal) they show more or less the same reduction. The wind speed is slightly lower in line 2 than in line 4, but not as much as we normally see in wake calculation models.


Wind speed vs. Turbine nr

L2_10_11 L4_10_11
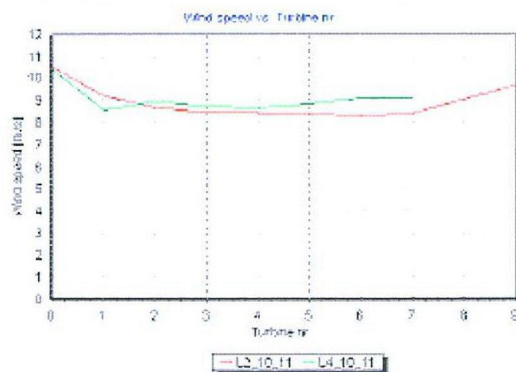
Turbulence intensity

The turbulence intensity along the lines has been investigated as well.

This is slightly trickier, since turbulence intensity is not calibrated on the nacelle anemometers. It is our general impression that the turbulence levels measured on the nacelle anemometers are smaller than those measured on the masts, and the masts are believed to be the more accurate.

Nevertheless, we find the plots rather interesting.

Windspeed 9 - 10 Wind dir: 268,4 - 271,4
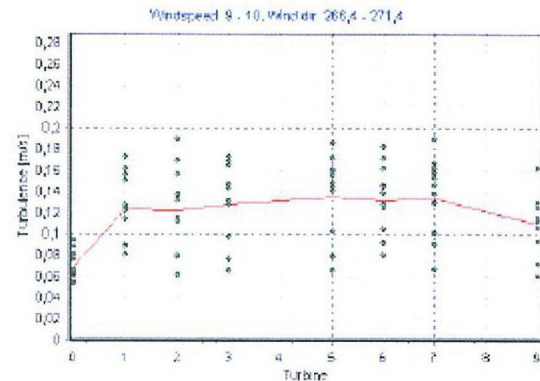
This graph shows the turbulence along line 2. It shows that generally there is an increase from the first to the second turbine, but further downstream the level is fairly constant. One interesting observation is that the spread of the recordings is fairly large, and the lower spots indicate that even in the 10th row, you can observe situations where the turbulence is not increased at all compared to the first turbine.

In line 4, the general tendency is the same. The turbulence level increases from the first to the second turbine, and is fairly constant for the turbines further downstream. It is noteworthy that the spread of the data is significantly smaller than in line 2 and that it does not show neither deep drops nor high peaks. Again this could be a consequence of merging wakes producing a more uniform flow pattern.
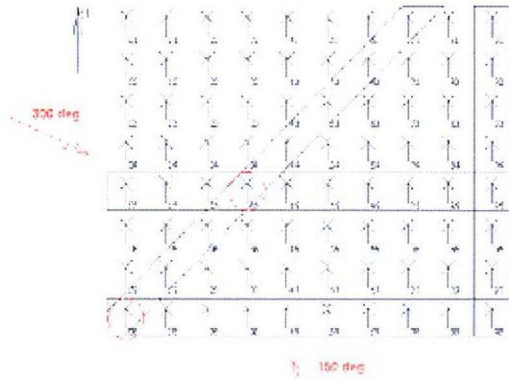

Windspeed 10 - 11 Wind dir: 217,89 - 222,89
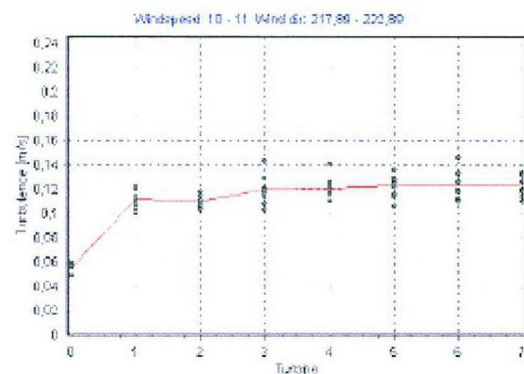
Directional dependence

To investigate the directional dependence of the wake effects, two turbines have been selected for further analysis.

The first turbine is no 35, which is located in the middle of the wind farm.

In this analysis we have taken the liberty of neglecting any effects of reduced availability of the wind farm. The only requirement in the data selection has been that turbine 08 at the southwest corner and turbine 35, being the object of analyses, were both in operation. The results shown should be viewed with that in mind. The absolute magnitude of the wind speed reduction cannot be trusted completely, but most likely the directional dependence will give a true picture.
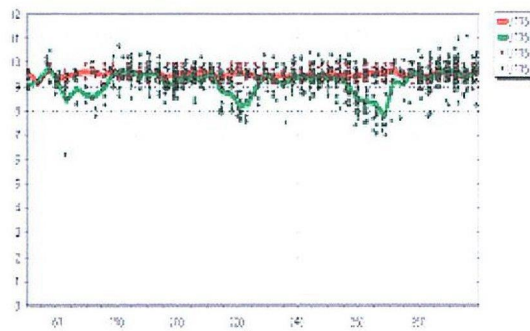
As indicated by the arrows on the layout chart above, the wind directions selected were from 150 to 300 degrees.

Both the aligned and the diagonal rows are seen clearly on turbine 35, and there appears to be practically no reduction in wind speed for intermediate wind directions.
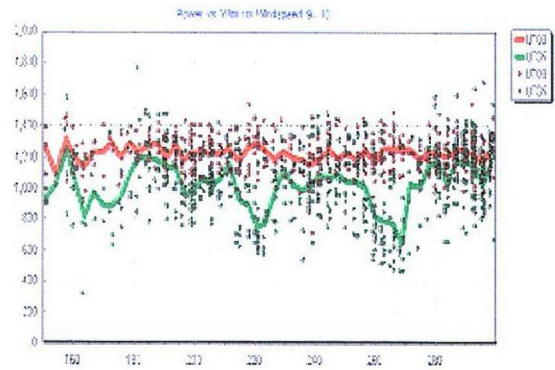
If wind turbine power output is observed instead of the wind speed of the nacelle anemometer, the largest reduction is still seen when the flow is aligned with the rows, but a small reduction is also seen for the intermediate wind directions.

The larger wake effect for intermediate wind directions seen on the power signal is probably partly due to the power output being significantly more sensitive than the wind speed, and partly because some parts of the rotor can easily be exposed to shelter from an upwind turbine even though the anemometer in the centre of the rotor is not.

The second turbine selected for directional dependence analysis is turbine 71.
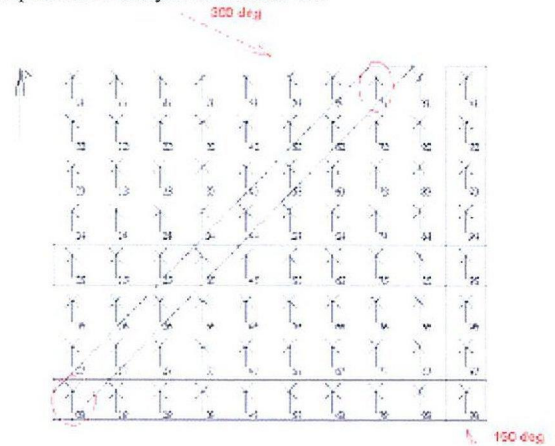
On this turbine, the individual lines are hardly seen. Wakes seem to have merged, forming a flow field that has no directional dependence.
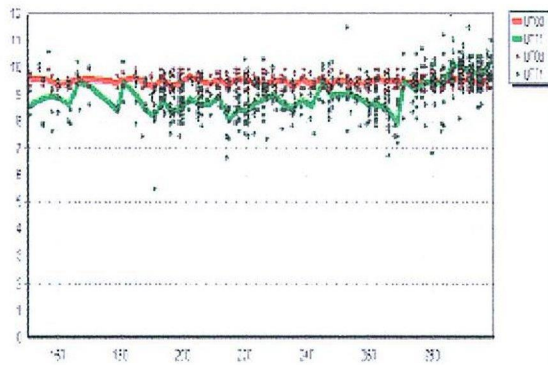
The most significant effect is from direction 270 and 300 where it is clear that both turbines are exposed to free wind, and wind speeds recorded are identical.
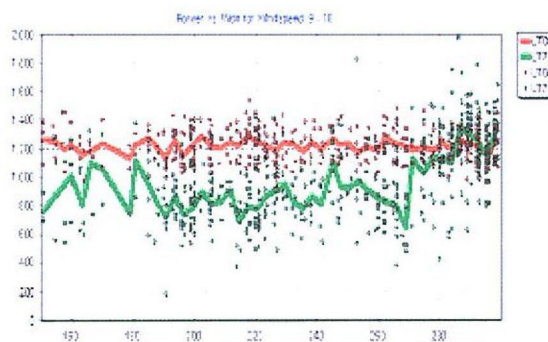
The tendency of the power output is the same, showing practically no special reduction for wind directions aligned with the turbine rows.

External wake effects
External wake effects can be studied using the results from the three met masts located around the wind farm.

The met masts have slightly different heights, but this is does not seem to have any significant influence on the observations made.

Hub height/top level	
Turbines	70
Mast 2	62
Mast 6	70
Mast 7	70

Met mast M6

For the analysis of the external wake effects, only wind speeds between 3 and 10 m/s have been selected.

As for the analysis of the directional dependence on wake effects, no sorting has been performed to get a well-defined availability, so this should be kept in mind for these results as well. The results are not suitable for detailed model calibrations yet, but they show some general tendencies.
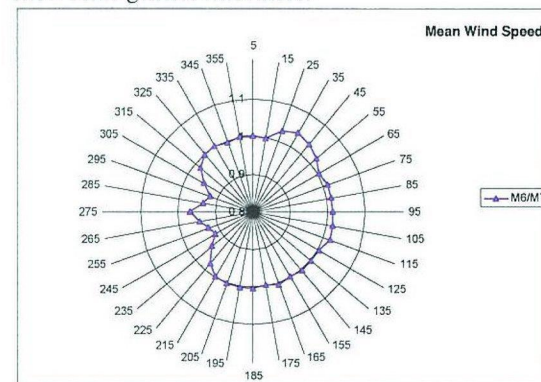

In this first graph, we have plotted the relation between the wind speed at masts M6 and M7. This means that for the westerly wind directions this graph shows the recovery of the wind speed from 2 to 6 km downstream.

It is noteworthy that the effect of the masts being installed between the turbine lines is seen so clearly for wind directions aligned with the turbine rows.

For wind directions between 20 and 50 degrees the influence of land is clearly seen on M7. For these wind directions, the flow towards M7 passes over the land at Blåvands Huk where M6 has a significantly larger fetch.

For wind directions between 50 and 120 degrees still a small influence of land is seen, indicating that the boundary layer flow has not yet changed completely to stable offshore conditions at this distance from shore.
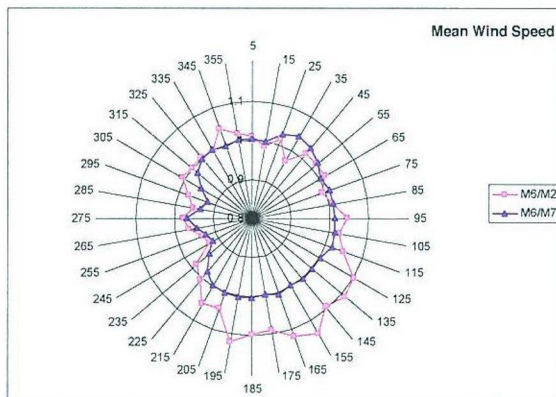

In this second graph we have added the relation between the wind speed at M6 and M2. This graph gives a clear picture of the wake effect on mast 2 for southeasterly winds, and confirms the reduced sheltering effect from wind directions aligned with the turbine rows.

Unfortunately, the plot also shows irregularities that cannot be explained at the present stage. For wind directions between northwest and east there seems to be good agreement between wind speed measurements on the two masts. But wind directions between south and northwest are not as expected.

For the directions 205 and 215 both M6 and M2 should be exposed to free inflow with no disturbances within a distance of hundred km. Nevertheless there is a difference in wind speed of 5%, which is about 5 times more than expected due to the vertical wind gradient. Also for the westerly directions it was to be expected that the reduction would be larger than what is actually measured when compared to M7.

By adding the relation between M7 and M2 to the plot (below) the irregularities become even more obvious. These measurements indicate that for westerly winds, the wind farm should lead to an increase in wind speed at a distance of 6 km downstream. We hope that a more careful study of possible disturbances from aviation obstruction lights and lightning protection will provide a reasonable explanation for that.
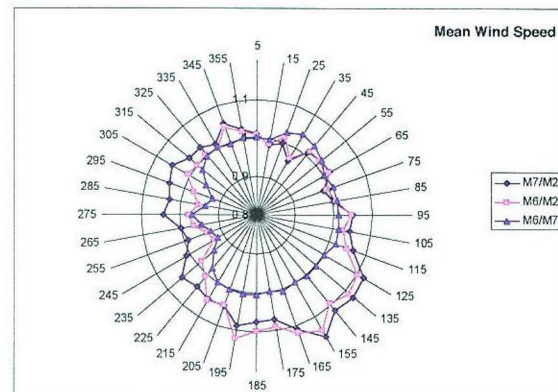
The assumption so far is that for wind directions between south and northwest there is a deviation in wind speed readings between the old mast (M2) and the new masts (M6 and M7) in the order of 4%. Whether it is M2 that is too low or M6 and M7 that are too high is presently unknown.

The turbulence intensity behind the wind farm has been investigated as well.
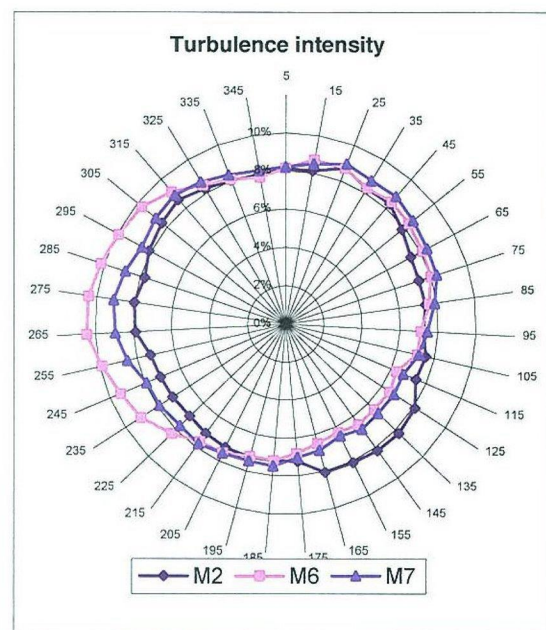
This plot shows the turbulence intensity recorded at M2, M6 and M7. Increased turbulence is seen on M2 for southeasterly winds.

When looking at turbulence data only from M2, the effect of the wind farm is almost hidden by the fact that the southeasterly winds have the lowest level of turbulence in the undisturbed conditions.

For easterly wind there is a clear (though very small) tendency showing that turbulence is higher on M7 than on M6 which could be a result of M7 being closer to land.

It appears that to obtain low turbulence offshore there is an optimum fetch where the disturbance from land has disappeared, and the waves have not yet been raised to a level that significantly influences the turbulence. For northeasterly winds where the fetch is smallest, there is still a clear effect of land on both mean wind speed and turbulence. For southeasterly winds where the fetch is 50 to 100 km, the turbulence level is the lowest, and for nothwesterly winds with waves coming all the way from the north of Scotland the turbulence level is high compared to the average.

For westerly winds the increase in turbulence on M6 and the recovery or relaxation of the flow towards M7 is very clear. The measurements clearly show that increased turbulence has not disappeared 6 km downstream of a large offshore wind farm.

It is noteworthy that the tunnelling effect of wind flow passing undisturbed between rows 4 and 5 is mainly a mean wind speed phenomenon. It is not seen on the turbulence plots at all.

Future R&D plans for the Horns Rev wind farm
In relation to wake effects, two future projects should be mentioned:

- Wake effects of large offshore wind farms
- Load measurements on turbine 14

Wake effects of large offshore wind farms is a Danish project involving Risoe National Laboratory, E2, with data from the Nysted offshore wind farm, and Elsam, with the Horns Rev data.

The project is funded by the Danish PSO system (Funds provided and administered by Eltra and Elkraft), and is scheduled to run from September 2004 to September 2006.

The main goal of the project is to develop new scientific and engineering models for calculation of wake effects of large offshore wind farms.

The load measurements on turbine 14 are a project presently involving only Vestas and Elsam. Activities were started during the summer of 2004, and measurements are expected to run for 9-12 months from December 2004.

The main goal of that project is to measure both the loads on nacelle and blades when operating in wake and free flow and to investigate loads transferred from the monopile to the seabed.

This project involves no public funding, and the measurement results are as such the property of Vestas and Elsam exclusively. Nevertheless the project expects to be able to provide useful data to public R&D projects on loads and wake effects for wind turbines in large offshore wind farms. This requires, however, that public funding is granted to

the scientific community for such work, and so far this has proven to be surprisingly difficult.

Further access to Horns Rev data
People from the scientific community often approach Elsam to get access to measurement data from the Horns Rev wind farm.

Our general policy on these matters is that we do whatever we can to help. However, in order to minimize the risk of spreading data that could directly or indirectly constitute information of commercial interest to Elsam or in any way reduce the competitive power of Elsam, we do not provide raw data for arbitrary analysis work.

Besides protecting the commercial interests of Elsam, we also believe that we can provide a better service by supplying processed data rather than raw data – simply because data processing requires a profound knowledge of details and irregularities in the wind farm operation (like the wind farm main controller).

This paper provides good examples of the kind of information that can be extracted from the SCADA system and the met masts. We believe that it will also provide most of the information needed to model the Horns Rev wind farm in wake calculation models.

If anybody wishes to model the Horns Rev wind farm and perform wake calculations, they are hereby invited to send us the results of their calculations. Then we will in return do our best to extract data that can confirm or reject the results of the model.

If you would like to learn more about the wake measurement analysis performed, you are very welcome to send an email to the lead author of this paper.